Università degli Studi di Padova

Dipartimento di Ingegneria dell'Informazione

Corso di Laurea in Ingegneria delle Telecomunicazioni

Analysis and Design of Self-Adapting Phased-Array Antennas on Conformal Surfaces

Laureando **Giulia Mansutti**

Relatore **Antonio Daniele Capobianco**

Anno Accademico 2014/2015

Contents

Abstract

This work deals with the study of conformal phased-array antennas, i.e. antennas designed to adapt to changing surfaces. When such surfaces modify their shape, the arrays placed on them deform as well, thus rising the issue of maintaining the overall antenna's radiation pattern.

The projection method is one of the possible solutions to this problem. Here this technique is applied to different conformal arrays, and through the comparison of the obtained results, advantages and drawbacks of this approach are pointed out. In particular in this work new conformal arrays were designed and studied through analytical investigation and numerical modeling, thus allowing further insights on the projection method and therefore providing an original contribution to this thesis.

Chapter 1

Introduction

Wireless systems have undergone huge developments in recent years, finding widespread applications: cellular networks, aviation communications, sensor networks, wearable devices, telemedicine are only some examples of technologies that rely on wireless systems. And a lot of other future applications will be based on them as well. For example the applications related to smart cities and more in general to the internet-of-things (IoT): vehicle-to-vehicle communications will improve safety and enable traffic control, intelligent and communicating household appliances will give the end-user the capability of monitoring and controlling their consumes, sensor networks can monitor a wide range of parameters, wearable technologies and telemedicine can improve people lifestyle [1].

These breakthrough applications are accompanied by stricter requirements like for example those that are depicted in the design of the 5G new standard for wireless communication [1] : diminished end-to-end latency (from 30-50 ms to 1 ms), higher throughput (from 100Mbps to

[1]No official draft of the requirements exists at the moment for 5G, but various telecommunications companies (e.g. samsung, huawei, ofcom) are outlining their own [2].

10Gbps), more connections per km^2 (from 10K to 1000K) and technology capable of functioning in high-mobility environments (e.g. high-speed railways 500km/h) [3] [2].

New requirements demand new improvements of consolidated technologies. Antennas are a good example of this process: they are one of the building blocks of wireless communications, and recently they have been the subject of novel scientific research that aims at providing them with new features in order to face present and future challenges.

Antenna systems are demanded for higher directivity, higher gains, and capability of functioning on changing surfaces in order to be placed for example on wearable devices that adapt to body movement [4] [5] [6], or on vibrating surfaces (for example on cars for vehicle-to-vehicle communication purposes) [7].

Conformal antennas phased-arrays have been gaining increasing attention by the scientific community as a feasible solution to this type of problems. Infact this type of antenna is capable of adapting to changing surfaces: the main challenge to face with this kind of phased-array consists in maintaining their original radiation pattern even when the surfaces on which they are placed, deform. In order to satisfy this requirement, various compensating techniques can be adopted: simple, cheap and easy to implement solutions exist and are subject of research, as well as more performing and complex ones. The choice of the particular technique depends on the final system's requirements and on the inevitable tradeoff between performance and ease of implementation.

In this work different configurations of conformal phased-arrays have been

designed and analyzed; in particular the projection method was applied as a pattern recovery technique and its improvements on the performance of the different conformal antennas were studied and compared. Moreover, some of the studied conformal arrays have been also prototyped and characterized in collaboration with the North Dakota State University, Fargo, ND, USA, with the goal of realizing a totally autonomous self-adapting system in the future.

Now, in order to present the study carried on in this thesis, it is useful to revise the work that has been done so far on conformal phased-arrays.

Previous Work

Antenna arrays, i.e. groups of several interconnected antennas arranged following some pattern in space, are used in order to increase the gain and directivity of a single element [8].

There are many possible geometrical configurations for the antenna elements that constitute an array: from the simplest one-dimensional linear array (Figure (1.1a), to various two- and three-dimensional configurations (Figure (1.1b-c) rispectively).

In a phased-array, differently from a single antenna, it is not necessary to vary the direction of the array in order to scan the radiation pattern, it is sufficient to change the phase of the currents that excite the single elements of the array. Thus an array has great advantages over a single antenna for example, the narrow main beam of a parabolic reflector antenna is scanned by slewing the entire structure, while arrays can be phase-scanned at the speed of the control electronics, without moving the entire structure. In addition it is possible to track multiple targets with an array. This is a great advantage and the reason why phased-arrays have become so popular in the

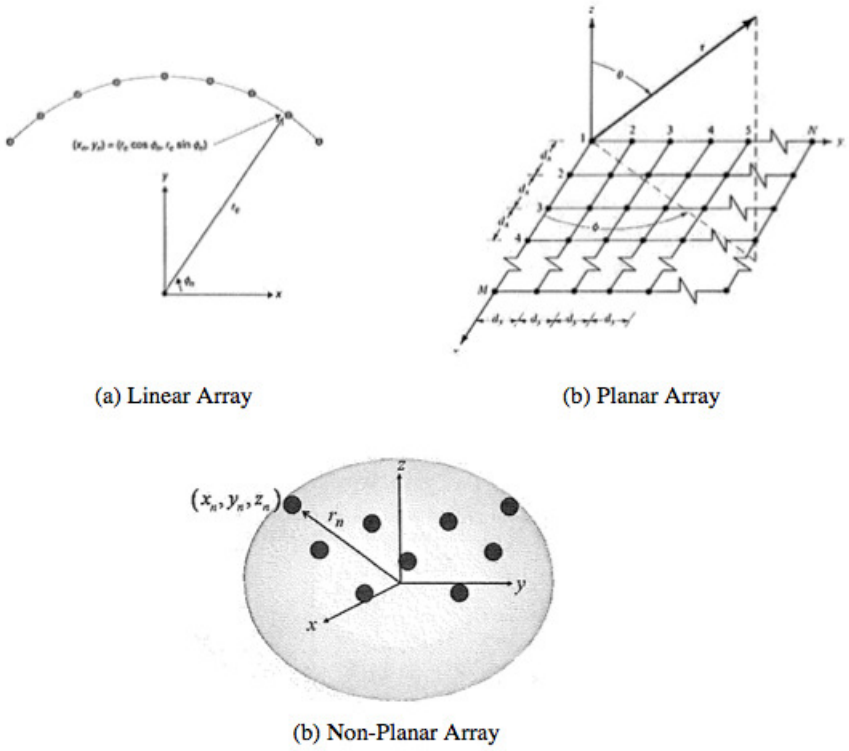

Figure 1.1: Different arrays: (a) linear, (b) planar, (c) non-planar.

aviation and military field, especially for radars.

The field of phased-array antennas was a very active area of research from the Second World War to about 1975. During this period, much pioneering work was done also for conformal arrays [9], i.e. an array designed to conform or follow some prescribed shape [10]. However, electronically scanned, phased array antennas did not find widespread use until the necessary means for feeding and steering the array became available. Integrated circuit (IC) technology including monolithic microwave integrated circuits (MMIC), filled this gap, providing reliable low cost solutions, even for complex array antennas.

An important factor was also the development of digital processors

that can handle the enormously increased rate of information provided by phased array systems. Digital processing techniques made phased array antenna systems cost effective. This being true for phased arrays in general, it also holds for conformal array antennas. However, in the area of conformal arrays, electromagnetic models and design know-how needed extra development: in the last 10 to 20 years, numerical techniques, electromagnetic analysis methods, and the understanding of antennas on curved surfaces have improved vastly [11], [12].

The origin of conformal arrays can be traced back at least to the 1930s when a system of dipole elements arranged on a circle, thus forming a circular array, was analyzed [13]. Later, in the 1950s, several pubblications on the subject were presented (for example [14]). The circular array was attractive because of its rotational symmetry and proper phasing can create a directional beam that can be scanned 360 degrees. The applications were in broadcasting communication and, later, navigation and direction finding.

A great deal of important conformal work was done at the U.S. Naval Electronics Laboratory Center (NELC) in San Diego. The work included development of both cylindrical and conical arrays as well as feeding system [9]. An indication of a recent resurgence in the interest in conformal antennas is the series of conformal antenna workshops, held in Europe every second year, starting in 1999.

In recent years, thanks to the development in electronics, the interest and studies on conformal arrays rose vastly. The main problem of an array placed on a conformal surface (i.e. that changes shape) lies in the fact that once the structure on which the antennas are placed, deforms, the radiation

pattern of the array changes as well. This brings to a reduction in the overall gain of the array, and in a diminished directivity of the system. In order to solve this issue, one of the most popular solutions [15] [16] [17] is based on the projection method [18]. This is a compensation technique that consists basically in projecting the single elements of the deformed array onto a reference plane, and then, through phase-tapering, in making the different signals from the single elements arriving in-phase on the new reference plane.

In [19] the projection method is used to recover the radiation pattern of a 1x4 conformal array placed on a non-conducting singly-curved wedge-shaped surface and on a non-conducting cylindrical-shaped surface. The various geometrical configurations are analyzed analytically (via matlab), by numerical simulation (via HFSS) and by measurement.

The first goal of this thesis is to retrace the results obtained in [19] both analytically and numerically, but making use of a different simulation software: CST Microwave Studio 2013.
Then the study and design of three novel conformal array antennas is presented, providing an original contribution to this work.
Finally the obtained results are compared in order to gain further insights on the projection method as a pattern recovery technique: its effectiveness is underlined as well as its drawbacks and limitations.

The following chapters will be organized as follows. Chapter 2 revises the most important theoretical concepts that have been used in this work, namely those regarding antenna arrays and patch antennas. Chapter 3 describes the model of the different conformal arrays studied in this work, focusing on the use of the projection method in each specific configuration. Chapter 4

presents the CST and matlab implementation of the system and the obtained results from the simulations. Finally Chapter 5 summarizes the conclusions of the work that has been done and the possible future implementations and developments.

Chapter 2

Background

In this thesis different configurations of conformal phased-arrays were designed and studied.

The various array configurations differ in the spatial distribution of the single elements, but they are all built with the same antennas, i.e. a rectangular microstrip patch resonating at 2.45GHz and fed by a 50Ω microstrip line.

In order to understand the analysis presented in the following chapters, it is first necessary to present some important theoretical concepts that were used to develop this work. Therefore, the aim of this chapter is to summarize the theory regarding the three building blocks of this thesis: phased arrays, conformal phased arrays and patch antennas.

2.1 Phased Antenna-Arrays

The radiation pattern of most antennas is usually relatively wide and presents low values of directivity and gain.

Many applications require antennas that can provide higher directivity

and narrow radiation pattern; in order to do so, a possible solution alternative to increasing the dimensions of a single antenna, consists in assembling various radiating elements in an electrical and geometrical configuration. Such a group of antennas is referred to as an *antenna array* [8].

A very popular choice is to build an array using identical antennas, as it has been done in this work. It's not a mandatory choice, but it is often convenient, simpler and more practical, therefore we will concentrate on this case.

The overall electric field radiated by the array is obtained by the vector addition of the single fields of each antenna. This holds under the hypothesis that there is *no mutual coupling* among the single antennas, or at least that coupling can be neglected: usually this is not true and in general it depends on the spatial distance among the elements.

In order to shape the overall pattern of the array, there are at least five parameters that can be controlled in an array of identical elements [8]:

1. the geometrical configuration of the array (e.g. linear, circular, spherical, etc.)
2. the relative displacement between consecutive elements;
3. the amplitude of the excitation signal of the individual elements;
4. the phase of the excitation signal of the individual elements;
5. the radiation pattern of the single elements;

The most simple array-configuration is obtained by placing the antennas along a line at equally spaced intervals, in this way we get a *linear array.* In this work, the initial undeformed array assumes this configuration,

consequently the next section describes the most important features of this type of array.

2.1.1 Two-Elements Linear Array

Let us consider a very simple array consisting of two infinitesimal dipoles positioned horizontally along the z-axis as depicted in Figure(2.1a).

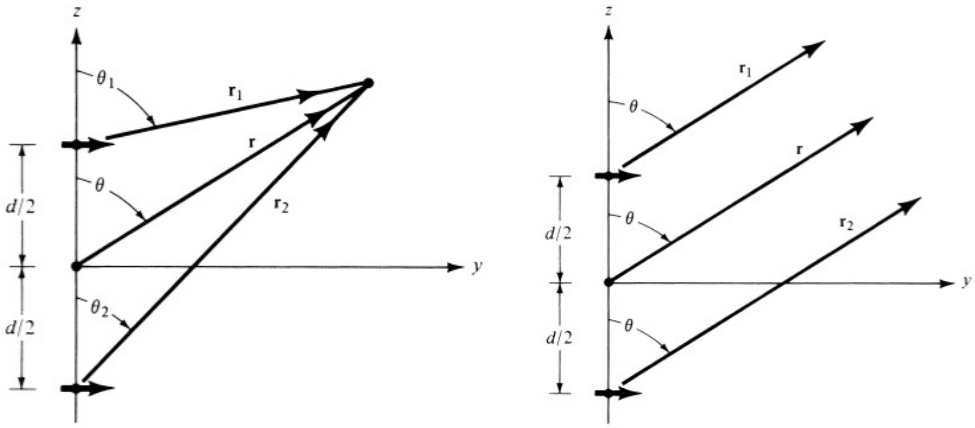

(a) Two dipoles array. (b) Farfield approximation.

Figure 2.1: Example of a linear two-element array [8].

Assuming no coupling between the two dipoles, the total electric field radiated by the array is given by the sum of the electric fields radiated by the two dipoles, and in the yz plane is given by:

$$\boldsymbol{E_{tot}} = \boldsymbol{E_1} + \boldsymbol{E_2} = \hat{\boldsymbol{a}}_{\vartheta} j\eta \frac{kI_0 l}{4\pi} \left\{ \frac{\exp^{-j[kr_1-(\beta/2)]}}{r_1} \cos\vartheta_1 + \frac{\exp^{-j[kr_2+(\beta/2)]}}{r_2} \cos\vartheta_2 \right\} \tag{2.1}$$

where $\hat{a}_{\vartheta} I_0$ is the spatial variation of the current that excites the dipole and I_0 is assumed to be constant, η is the wave impedance, l is the length of the dipole, r_1 and r_2 are the distances of the two dipoles from the observation

point, k is the wave vector, ϑ_1 and ϑ_2 are the angles between r_i and the $z-$axis and β is the phase difference between the currents that excite the two dipoles.

Assuming farfield observation we can make these simplifications (see Figure(2.1b)):

$$\vartheta_1 \simeq \vartheta_2 \simeq \vartheta\,, \tag{2.2}$$

$$r_1 \simeq r - \frac{d}{2}\cos\vartheta\,, \qquad r_2 \simeq r + \frac{d}{2}\cos\vartheta \tag{2.3}$$

$$r_1 \simeq r_2 \simeq r \tag{2.4}$$

where (2.3) is used when dealing with phase variations while (2.4) is used with amplitude variations. Thus, equation (2.1) reduces to:

$$\boldsymbol{E_{tot}} = \hat{\boldsymbol{a}}_{\boldsymbol{\vartheta}} j\eta \frac{kI_0 l \exp^{-jkr}}{4\pi r}\cos\vartheta\Big\{2\cos\Big[\frac{1}{2}(kd\cos\vartheta+\beta)\Big]\Big\} \tag{2.5}$$

So the total field of the array is the product between the field radiated by a single element of the array positioned in the origin (i.e. the term before the graph parenthesis in Eq.(2.5)) and a term that is known as the *array factor*:

$$AF = 2\cos\Big[\frac{1}{2}(kd\cos\vartheta+\beta)\Big] \tag{2.6}$$

or in normalized form:

$$(AF)_n = \cos\Big[\frac{1}{2}(kd\cos\vartheta+\beta)\Big] \tag{2.7}$$

The AF is a function of the spacing d between adjacent elements in the array and the phase difference β in the excitations of the two elements.

It has been shown that the total radiated field by an array is given by the product of the field of a single element, at a selected reference point

(usually the origin), and the array factor of that array. This is referred to as *pattern multiplication* for array of identical elements [8].

2.1.2 N-elements Uniform Linear Array

The method presented above can be generalized to the general case of a uniform N-elments array.

Definition An array of identical and equally spaced elements all of identical magnitude and each with a progressive phase, is referred to as a uniform array.

Since pattern multiplication applies to this type of array, the total radiated field is given by the sum of the fields radiated by the single elements, or equivalently by the product of the AF and the field radiated by a single element placed in the reference point (usually the origin).

In an identical manner as what have been done for the case of a two-elements array, we can make farfield approximations similar to those of Eq. (2.2)(2.3)(2.4) (see Figure(2.2)). In this way we can evaluate the AF as:

$$AF = 1 + e^{j(kd\cos\vartheta+\beta)} + e^{j2(kd\cos\vartheta+\beta)} + \cdots + e^{j(N-1)(kd\cos\vartheta+\beta)} = \\ = \sum_{n=1}^{N} e^{j(n-1)(kd\cos\vartheta+\beta)}$$

which can be written as:

$$AF = \sum_{n=1}^{N} e^{j(n-1)\psi} \ , \qquad \psi = kd\cos\vartheta + \beta \tag{2.8}$$

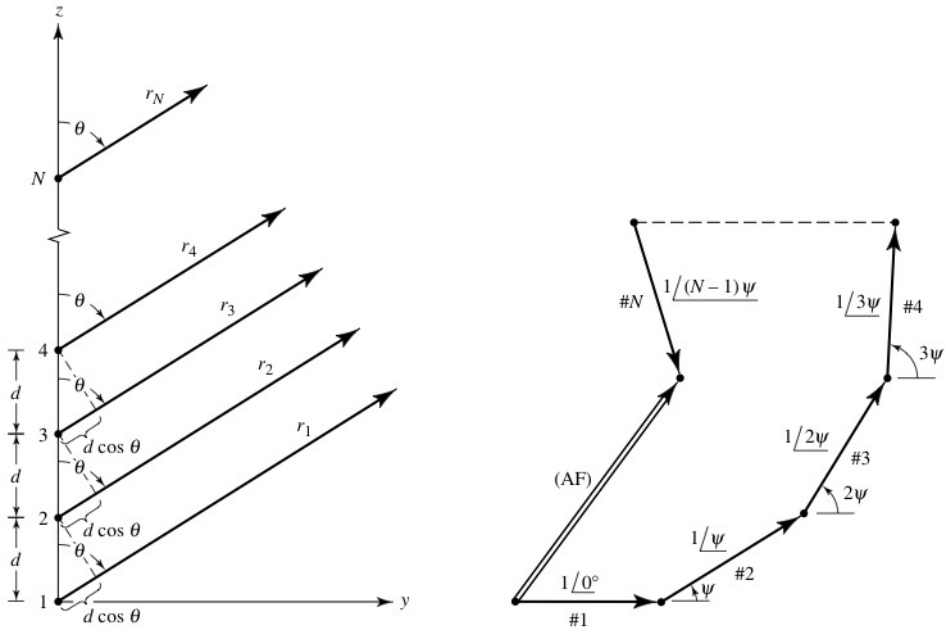

Figure 2.2: Array of N elements and their phasors [8].

Therefore, since the total AF is a summation of exponentials, it can be represented by phasors as depicted in Figure(2.2) and it can be also expressed in an alternate compact and closed form. Multiplying both sides of (2.8) by $e^{j\psi}$ we get:

$$(AF)e^{j\psi} = e^{j\psi} + e^{j2\psi} + \cdots + e^{j(N-1)\psi} + e^{jN\psi} \tag{2.9}$$

and subtracting (2.8) this:

$$AF = \left[\frac{e^{jN\psi} - 1}{e^{j\psi} - 1}\right] = e^{j[(N-1)/2]\psi}\left[\frac{e^{j(N/2)\psi} - e^{-j(N/2)\psi}}{e^{j(1/2)\psi} - e^{-j(1/2)\psi}}\right] = \tag{2.10}$$

$$= e^{j[(N-1)/2]\psi}\left[\frac{\sin\left(\frac{N}{2}\psi\right)}{\sin\left(\frac{1}{2}\psi\right)}\right] \tag{2.11}$$

If we choose the physical center of the array (e.g. the middle point of

the line on which the antennas are placed in a linear array) as the reference point, this expression reduces to:

$$AF = \left[\frac{\sin\left(\frac{N}{2}\psi\right)}{\sin\left(\frac{1}{2}\psi\right)}\right], \qquad \psi = kd\cos\vartheta + \beta \tag{2.12}$$

From this expression this expression we can make some considerations:

- The maximum value of the AF is N. In fact, for $\psi \to 0$, we can replace the sine with its first-order Taylor approximation [1] , thus getting:

$$AF = \left[\frac{\sin\left(\frac{N}{2}\psi\right)}{\sin\left(\frac{1}{2}\psi\right)}\right] \simeq \frac{\frac{N}{2}\psi}{\frac{1}{2}\psi} = N \tag{2.13}$$

  this means that combining N antennas in an array can increase the overall gain of a factor N.

- The maximum value for the AF is achieved when the argument of both the numerator and the denominator goes to zero, that is when $\psi = 0$, in correspondence of this value we can find the main lobe (principal maximum) of the AF. Other maxima can be found for $\psi = \pm m\pi$ and in correspondence of these values we can find the grating lobes of the AF (secondary maxima). In general a lobe (main or grating) can be found when:

[1] The first-order approximation of the sine function for $x \to 0$ is given by: $\sin(x) = x + o(x)$, where $o(x)$ is any function $f(x)$ such that $\lim_{x\to 0} \frac{f(x)}{x} \to 0$.

$$\sin\Big(\frac{\psi}{2}\Big) = 0 \quad \Rightarrow \quad \frac{\psi}{2} = \pm m\pi \quad \Rightarrow \quad kd\cos\vartheta + \beta = \pm m\pi \tag{2.14}$$

$$\vartheta_m = \cos^{-1}\Big[\frac{1}{kd}\Big(-\beta \pm 2m\pi\Big)\Big] \tag{2.15}$$

$$m = 0,\, 1,\, 2,\, \ldots \tag{2.16}$$

For $m = 0$ we get the main lobe, while for the other values we get the grating lobes.

- The AF assumes null values when the numerator of (2.13) is zero, i.e. when:

$$\sin\Big(\frac{N}{2}\psi\Big) = 0 \quad \Rightarrow \quad \frac{N}{2}\psi = \pm n\pi \quad \Rightarrow \quad kd\cos\vartheta + \beta = \pm n\pi \tag{2.17}$$

$$\vartheta_n = \cos^{-1}\Big[\frac{1}{kd}\Big(-\beta \pm \frac{2n}{N}\pi\Big)\Big] \tag{2.18}$$

$$n = 1, 2, \ldots \qquad n \neq N,\, 2N, \ldots \tag{2.19}$$

Controlling the parameters of the array enables to set some features like for example the main lobe's direction, the number of grating lobes and the positions of the nulls.

In many applications (and in this work too) it is desirable to have the main lobe perpendicular to the array, i.e. in the $\vartheta = 90°$ direction (see Figure(2.2)). In order to do so, Eq.(2.14) is set accordingly:

$$\psi \Big|_{\vartheta=90°} = kd\cos\vartheta + \beta \Big|_{\vartheta=90°} = \beta = 0 \tag{2.20}$$

So this condition reduces to imposing the same phase on the exciting

currents of all the elements of the array, no condition on the distance among the elements is imposed.

Usually it is desirable not to have grating lobes. This condition is satisfied imposing:

$$\psi \Big|_{\beta=0} = kd\cos\vartheta \neq \pm 2n\pi \quad \forall\vartheta \quad \Rightarrow \quad d\cos\vartheta \neq \pm 2n\pi\frac{\lambda}{2\pi} \neq \pm n\lambda \quad n = 1, 2, \ldots \tag{2.21}$$

So, since $d\cos\vartheta \leq d$, the condition under which no grating lobes exist becomes $d \leq \lambda$.

From this section it is clear that by changing the parameters of a uniform array, such as the spacing and the phase difference between the elements, some requirements can be satisfied: for example the direction of the maximum and nulls's positions can be set and the number of grating lobes can be controlled.

The next section investigates the theory about the central topic of this work: conformal arrays.

2.1.3 Conformal Arrays

In order to better understand this section that deals with the the deformation of a linear array, it is useful to introduce a convenient mathematical description for the three-dimensional characteristics of an N-elements linear array.

Up to now the two-dimensional array factor has been considered. In Figure(2.2) the N-elements array is positioned along the z-axis and the

observation point is placed in the yz plane. However, it's useful to get a more general expression for the AF that comprises the case in which the observation point is any point of space.

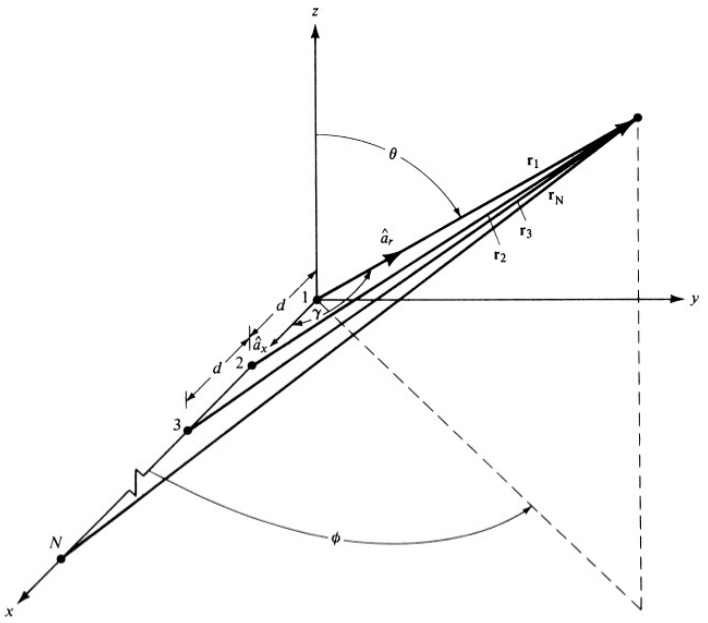

Figure 2.3: Spherical coordinate system for an N-elements linear array [20].

Let us consider again an N-elements linear array positioned along the z-axis, but this time the observation point doesn't lie in the yz plane, as depicted in Figure(2.3). A spherical coordinate system is adopted: r is the distance of the observation point from the origin, φ is the azimuthal angle and ϑ is the elevation angle.

In this case the array factor is given by:

$$AF = \sum_{n=1}^{N} w_n e^{j\psi_n} \tag{2.22}$$

where $w_n = a_n e^{j\delta_n}$ is the complex weight for element n and it comprises the amplitude and phase of the n-th exciting current and ψ_n depends on which

axis the array lays on:

$$\psi_n = \begin{cases} kx_n \cos\varphi & or \quad kx_n \sin\vartheta & x\text{-}axis \\ ky_n \sin\varphi & or \quad ky_n \sin\vartheta & y\text{-}axis \\ kz_n \cos\vartheta & & z\text{-}axis \end{cases} \tag{2.23}$$

Now if we consider a general planar array (Fig.(2.4)) with the elements placed on one of the tree planes xy, xz or yz, the expression of the AF is the same of (3.3), except for ψ_n that now becomes:

$$\psi_n = \begin{cases} k(x_n u + y_n v) & xy\ plane \\ k(x_n u + z_n w) & xz\ plane \\ k(y_n u + z_n w) & yz\ plane \end{cases} \tag{2.24}$$

where (x_n, y_n) is the location of element n, $u = \sin\vartheta\cos\varphi$, $v = \sin\vartheta\sin\varphi$ and $w = \cos\vartheta$.

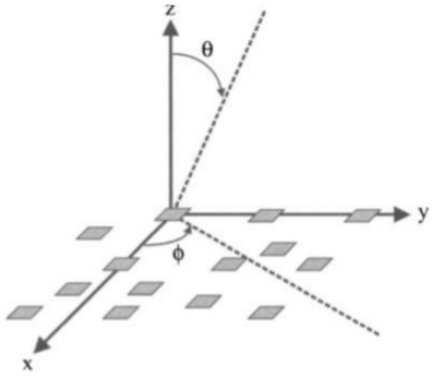

Figure 2.4: Planar array and associated coordinate system [20].

This work deals with *conformal arrays*, i.e. arrays placed on surfaces that change shapes. So it's important to introduce the expression for the AF in

the case of a generic non-planar array like the one depicted in Figure(2.5).

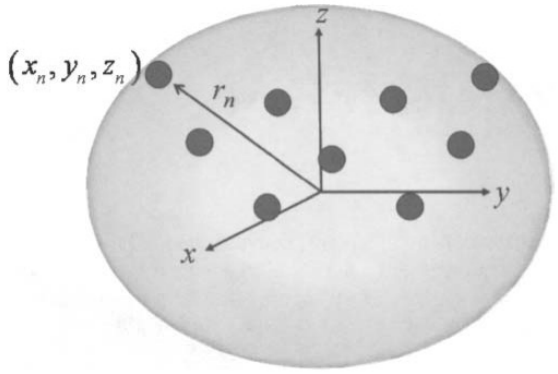

Figure 2.5: Non-planar array and associated coordinate system [20].

In this case the array factor is given by:

$$AF = \sum_{n=1}^{N} e^{jk[x_n(u-u_s)+y_n(v-v_s)+z_n \cos\vartheta]} \tag{2.25}$$

where $u = \sin\vartheta\cos\varphi$, $u_s = \sin\vartheta_s\cos\varphi_s$, $v = \sin\vartheta\sin\varphi$, $v_s = \sin\vartheta_s\sin\varphi_s$ and ϑ_s and φ_s are again the elevation steering angle and the azimuth steering angle respectively.

The Projection Method

All these considerations are essential in order to define a strategy to recover the pattern of an array placed on a deformed surface, i.e. of a conformal array. Infact the main characteristics of an array, like gain and directivity, are affected from the deformation of the array. In [20] and also in this work is shown that the performance of a bent array degrade: directivity is lower and side lobes grow greater.

For the purpose of this work, we will focus on arrays placed on conformal singly-curved surfaces. Two examples of this type of arrays are presented in

Figure(2.6). Fig.(2.6a) depicts a linear array deformed on a wedge surface bent of ϑ_b degrees with respect to the x-axis, while in Fig.(2.6b) a linear array bent on an arc of circumference is depicted. These two types of arrays have been studied in [19] and also in this work, therefore they will be used as the examples to introduce the issues and solutions related to the deformation of a linear array.

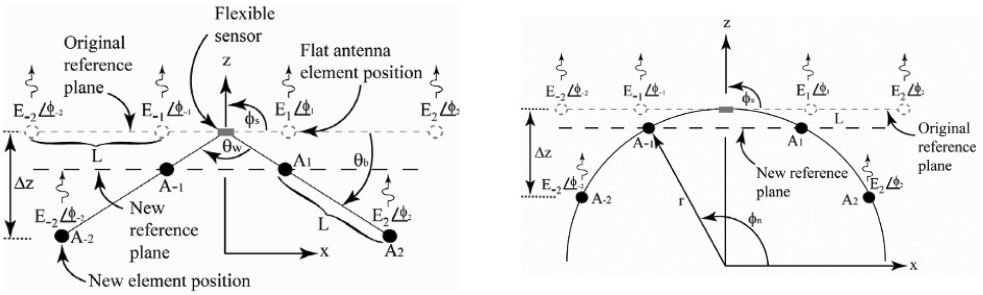

(a) Wedge surface deformation.

(b) Arc surface deformation.

Figure 2.6: Examples of conformal array: bent on a wedge surface (2.6a) and on an arc of circumference (2.6b) [19].

A strategy to mitigate the problems connected to the deformation of an array has been introduced in [18] and it is known as the *projection method*. According to this strategy, the main cause of performance degradation lays in the fact that, since the elements of the array are misplaced with respect to their original position, when the different signals reach the observation point, their relative phase-difference isn't the same of the original undeformed array: in some points where the signals were supposed to interact constructively they instead interact destructively, and vice versa.

Thus, the projection method consists basically in introducing a proper phase-compensation in order to restore the original relative phase-difference among the signals arriving at the observation point. Considering a linear

array originally placed on the x-axis, like those of Figure(2.6), the basic steps in order to introduce the compensating phase-shifts are the following:

1. Draw a new (imaginary) reference plane, orthogonal to the steering direction of the original array;

2. Project the elements of the deformed array onto the new reference plane, with the projection lines parallel to the original steering direction;

3. For each element set the proper phase-shift compensation:

$$\delta_n = -k(|x_n| \cos \varphi_s + |z_n| \sin \varphi_s) \tag{2.26}$$

This equation represents the general form of the compensating phase-shift, i.e. it includes the cases in which the main lobe is steered at an angle different from 90° (non-broadside array) as studied in [21], [22] and as represented in Figure(2.7).

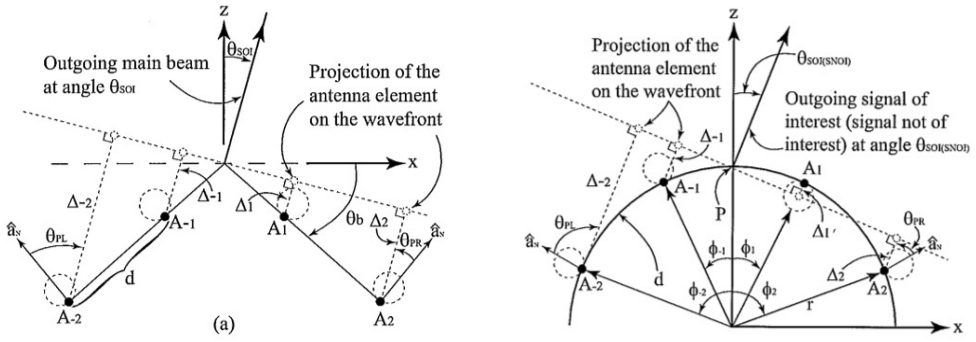

(a) Wedge surface deformation. (b) Arc surface deformation.

Figure 2.7: Conformal arrays with non-broadside beam [19].

If we limit our attention to the case of broadside radiation ($\varphi_s = 90°$ as in Figure(2.6)), the required phase-shift δ_n for the n-th element simplifies to:

$$\delta_n = -k|z_n| \tag{2.27}$$

Moreover if the new reference plane doesn't coincide with the x-axis, but it is simply parallel to it and consists of the horizontal line that comprehend the elements nearest to the x-axis (see Figure(2.6)), then we can write:

$$\delta_n = -k|\Delta z_n| = -k\ |z_n - z_{ref}| = \begin{cases} kL(|n|-1)\sin\vartheta_b & \textit{wedge} \\ kr|\sin\varphi_{n+1} - \sin\varphi_n| & \textit{arc} \end{cases} \tag{2.28}$$

where z_{ref} is the z-ordinate of the reference plane, L is the original spacing between the elements of the linear array, r is the radius of the shaping circumference, φ_n is the angle formed by the vector connecting the n-th element to the origin with the x-axis and the elements are numbered $-N/2, \ldots, -1$ from right to left in the second quadrant and $1, \ldots, N/2$ from left to right in the first quadrant [2]. The phase shift is introduced for all the elements except for those lying on the new reference plane. Basically $L(|n|-1)\sin\vartheta_b$ and $r|\sin\varphi_{n+1} - \sin\varphi_n|$ are the distances of the n-th element from the new reference plane when the array assumes respectively a wedge form and an arc form.

There is one last topic to address regarding conformal arrays and pattern recovery. In almost all the arrays, the element pattern peak is normal to the surface of the antenna (this is the case of patch antennas for example), so when the array is placed on a conformal surface and this surface deforms, the peaks of the single elements become normal to the conformal surface.

[2] This holds for an even number of elements; if there is an odd number of elements the central element (that is placed in correspondence of the origin) is numbered zero

When the single elements are isotropic sources (they irradiate uniformly in all the directions, as for example a dipole does) and the array is bent, the total radiation is computed by the product of the AF and the radiation pattern of a single element. The same is done when the single elements's radiation peak is normal to the antenna and the array is linear. But when the element pattern peak is normal to the surface of the antenna and the array is bent (Figure(2.8)), the computation of the total radiated field becomes more complex and an additional term $e(\vartheta - \vartheta_n)$ must be included in the AF:

$$AF = \sum_{n=1}^{N} e(\vartheta - \vartheta_n) w_n e^{jk[x_n \sin\vartheta\cos\varphi + y_n \sin\vartheta\sin\varphi + z_n\cos\vartheta]} \tag{2.29}$$

where $e(\vartheta - \vartheta_n)$ is the element pattern of element n having a peak at $\varphi = 0°$. So now the antenna pattern is not the product of a single element pattern times an array factor. This must be taken into considerations and will be useful in the next chapters.

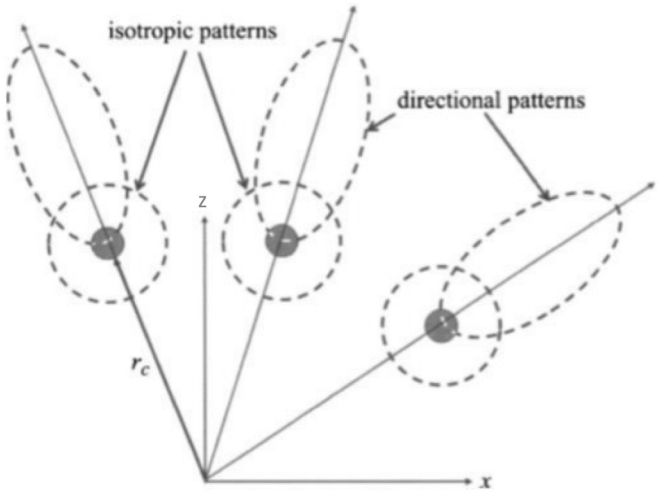

Figure 2.8: Comparison of a conformal array with directional elements to one with isotropic elements [20].

In this section some important features of antennas-arrays and conformal

arrays were investigated. The next section describes instead some important properties of the antennas used as the single elements in this work: patch antennas.

2.2 Patch Antennas

The idea of a microstrip antenna can be traced back to 1953, even though this type of antennas received considerable attention only years later starting from the 1970s [23].

Microstrip antennas possess many desirable characteristics: they are low-profile, conformable to planar and non-planar surfaces, simple and cheap to manufacture (thanks to modern printed-circuit technology), compatible with MMIC design (Monolithic Microwave Integrated Circuit), mechanically robust when mounted on rigid surfaces, and, once the particular patch shape and mode are selected, they are very versatile in terms of resonant frequency, polarization, pattern and impedance.

For this reasons microstrip antennas are an appealing solution for many applications subject to strict requirements regarding size, weight, cost, performance, ease of installation and aerodynamic profile. For example: spacecraft, aircraft, satellite and missile applications, but also commercial ones such as mobile radio and wireless communications [8].

On the other side microstrip antennas show also disadvantages, the major being their low efficiency, low power, high Q, poor scan performance, spurious feed radiation and very narrow frequency bandwidth (typically a fraction of a percent or at most a few percent). However there are various methods to mitigate these drawbacks, even if this topic isn't addressed in this work.

2.2.1 Basic Characteristics

A microstrip antenna is a broadside radiator (i.e. it is designed in such a way that its pattern maximum is normal to the patch) that consists of a very thin metallic patch ($t \ll \lambda_0$, with λ_0 being the free-space wavelength) placed at a small distance above a ground plane ($h \ll \lambda_0$, usually $0.03\lambda_0 \leq h \leq 0.05\lambda_0$), as can be seen from Figure(4.1).

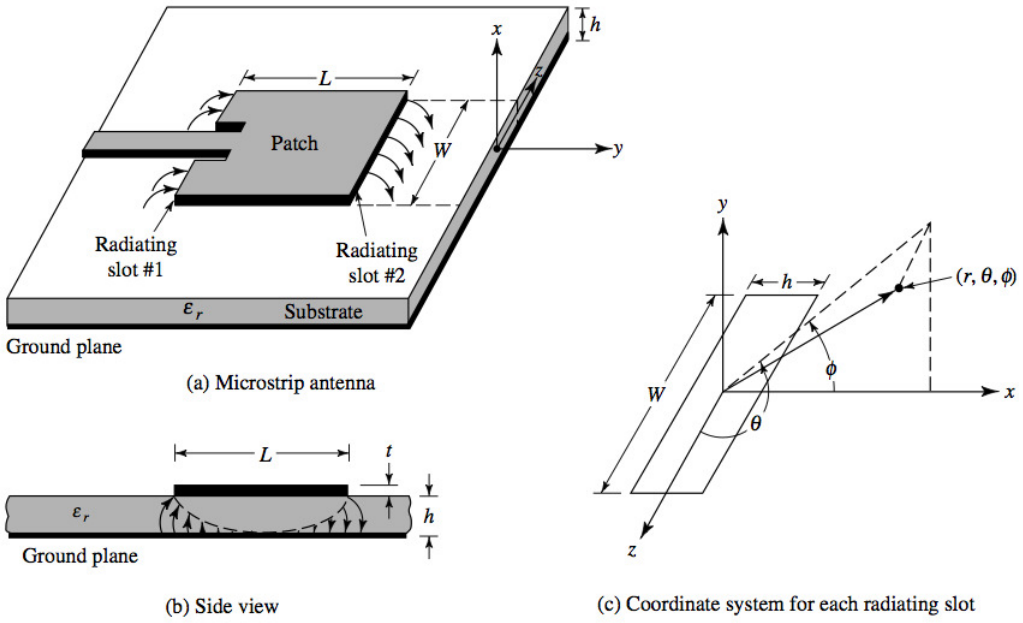

Figure 2.9: Microstrip antenna and coordinate system [8].

The patch and the ground plane are separated by a substrate that can be of various materials, but typically its dielectric constant lies in the range $2.2 \leq \varepsilon_r \leq 12$ [8].

A patch antenna is a broadside radiator, i.e. it is designed in order for its pattern maximum to be normal to the patch. As it's shown in Figure(2.10) the radiating patch may be designed according to different shapes: the most popular ones are square, rectangular and dipole because of their ease of

analysis and fabrication. This chapter describes the characteristics only of the rectangular one, since this is the shape that has been chosen to design the single elements of all the array configurations analyzed in this work.

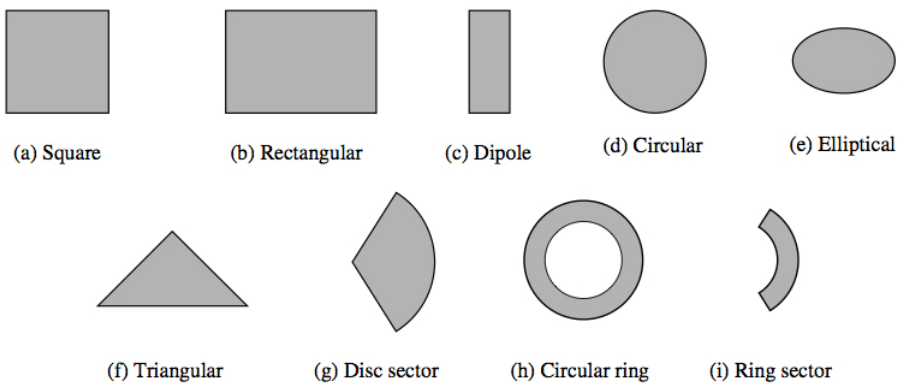

Figure 2.10: Some possible shapes for microstrip patch elements [8].

As far as the feeding technique of the patch is concerned, there are mainly four configurations (depicted in Figure(2.11)): microstrip line, coaxial probe, aperture coupling and proximity coupling.

In this work a microstrip line feed has been used: this configuration owes its popularity to the ease of modeling and fabrication, and to the simplicity of impedance matching: in order to do so, it is sufficient to control the inset position.

Another popular configuration is the coaxial-line feed, where the inner conductor is connected to the radiation patch, while the outer conductor is attached to the ground plane. In both these configurations however, as the substrate's thickness increases, also the surface waves increase, thus limiting the bandwidth; moreover due to asymmetries higher-order modes are generated which produce cross-polarized radiation. Aperture-coupled and proximity-coupled feed have been introduced to overcome some of these

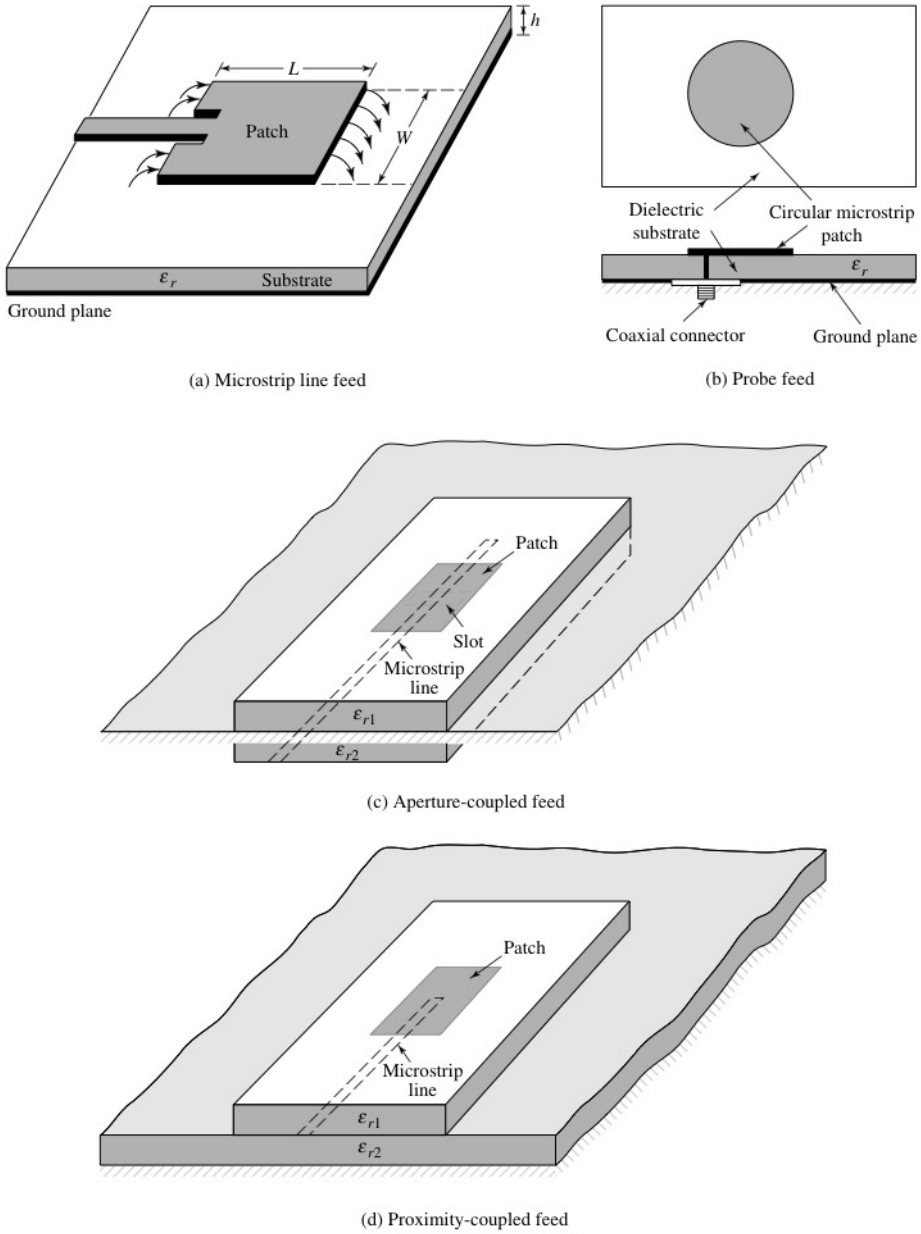

Figure 2.11: Different feeding techniques for a patch antenna [8].

problems.

In this work however, the adopted feeding technique is the microstrip-line, so the following analysis involves just this configuration.

2.2.2 The transmission line model

The analysis methods for microstrip antennas are manifold. The most popular ones are the transmission-line, cavity and full-wave models. The transmission-line is the simplest one: it provides good physical insight but it's less accurate and not very suitable to model coupling. The cavity model is more accurate but also more complex; the full-wave model, that is based primarily on integral equations, is very accurate and very versatile, but it's also much more complex and not very useful to gain physical insight.

Therefore the rectangular patch antenna is analyzed here through the transmission-line model. According to this model, the patch antenna is represented as an array of two radiating slots of width W and height h, separated by a low-impedance transmission line of length L.

Fringing

The finite dimensions of the patch along the length and width cause the field at the edges to undergo fringing, as it's shown in Figure(2.11)(a). The entity of the fringing phenomenum depends on the ratio L/h between the length of the patch and th and the height of the substrate and on the ratio W/h between the width of the patch and h. Since it is $L/h \gg 1$ and $W/h \gg 1$, the effect of fringing is reduced, but not so much to be negligible and therefore it must be taken into account since it affects the resonant frequency of the antenna.

Figure(2.12)(b) shows a representation of typical electric field lines for a microstrip line (Figure (2.12)(a)), that is a nonhomogeneous line of two dielectrics (the substrate and air). As it can be seen from the figure, the fact that $W/h \gg 1$ and $\varepsilon_r \gg 1$ cause the majority of the field lines to concentrate in the substrate.

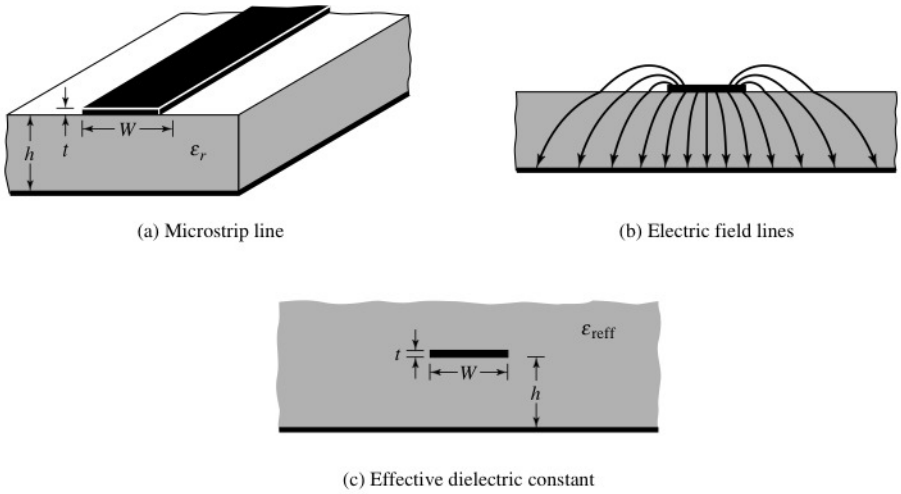

Figure 2.12: Microstrip line (a), the effect of fringing on its electric field line (b) and graphical representation of the effective dielectric constant [8].

It is useful now to introduce the *effective dielectric constant* ε_{reff}. This is the dielectric constant of the fictitious uniform dielectric material that surrounds the microstrip line in Figure(2.12)(c) so that the line has identical electrical characteristics, in particular propagation constant, as the actual line of Figure(2.12)(a).

The effective dielectric constant has some properties:

- For a line with air above the substrate it holds $1 < \varepsilon_{reff} < \varepsilon_r$; for most application where $\varepsilon_r \gg 1$, ε_{reff} assumes values near ε_r;
- It is a function of frequency: as the frequency of operation grows, the electric field lines concentrates more and more in the substrate leading to an effective dielectric constant that approaches the constant of the dielectric;

- For low frequencies ε_{reff} is almost constant and the initial value (also called static value) of ε_{reff} is given by:

$$\varepsilon_{reff} = \frac{\varepsilon_r + 1}{2} + \frac{\varepsilon_r - 1}{2}\left[1 + 12\frac{h}{W}\right]^{-\frac{1}{2}} \qquad W/h \gg 1 \qquad (2.30)$$

Effective Length, Resonant Frequency and Effective Width

Due to the fringing effects, the patch of the microstrip antenna looks bigger (electrically) than its physical dimensions. A graphical representation of this effect is reported in Figure(2.13), from where it can be seen that the patch length is increased of a factor $2\Delta L$, where ΔL is a function of the ratio W/h between the width of the patch and the height of the substrate and of the effective dielectric constant ε_{reff}.

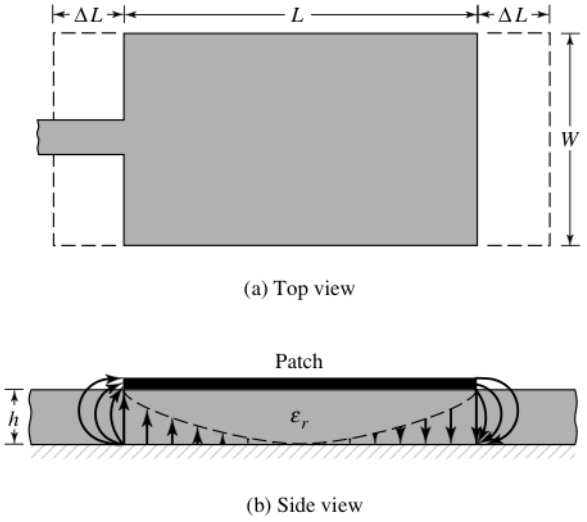

Figure 2.13: Physical and effective lengths of a rectangular microstrip patch [8].

A popular and practical approximate expression for ΔL is given by [24] that leads to an effective length of the patch L_{eff} of:

$$\Delta L = 0.142h\frac{(\varepsilon_{reff}+0.3)\left(\frac{W}{h}+0.264\right)}{(\varepsilon_{reff}-0.258)\left(\frac{W}{h}+0.8\right)} \tag{2.31}$$

$$L_{eff} = L + 2\Delta L \tag{2.32}$$

Usually the resonant frequency for the microstrip antenna is a function of its length and for the dominant TM_{010} mode (quasi-TEM) is given by:

$$f_{r,010} = \frac{1}{2L\sqrt{\varepsilon_r}\sqrt{\mu_0\varepsilon_0}} = \frac{c_0}{2L\sqrt{\varepsilon_r}} \tag{2.33}$$

with c_0 being the speed of light in free space. But taking into account fringing effects, (2.33) becomes:

$$f_{r,010} = \frac{1}{2L_{eff}\sqrt{\varepsilon_{reff}}\sqrt{\mu_0\varepsilon_0}} = \frac{c_0}{2L_{eff}\sqrt{\varepsilon_{reff}}} \tag{2.34}$$

Design

As reported in [8] a simple procedure to design a rectangular patch antenna is the following.

The goal is to determine the width W and length L of the patch (see Figure(4.1)) in order to match the desired resonant frequency f_r, given the substrate's dielectric constant ε_r and height h.

The design procedure follows these steps:

1. First the width of the radiator is determined according to this practical formula that leads to good efficiencies [25]:

$$W = \frac{c_0}{2f_r}\sqrt{\frac{2}{\varepsilon_r+1}} \tag{2.35}$$

2 Then the effective dielectric constant is determined using (2.30)

3 Now given W and ε_{reff}, ΔL can be determined using (2.31)

4 Finally the actual length of the patch is given by:

$$L = \frac{c_0}{2f_r\sqrt{\varepsilon_{reff}}} - 2\Delta L \tag{2.36}$$

As far as the input resistance is concerned, we limit our discussion stating what is explained in detail in [8]: the resonant input resistance of the patch can be changed by using an inset feed that is recessed at a distance y_0 from the bottom of the patch, as shown in Figure(2.14).

From Figure(2.14)(b) it can be seen how changing y_0 allows matching the patch antenna.

As stated before, patch antennas present many advantages but also some drawbacks, among which poor scan performance and narrow bandwidth. In order to overcome or at least mitigate some these two problems, multiple microstrip antennas can be arranged in space and fed by precise input signals. The following section will revise some of the most important theoretical concepts regarding arrays.

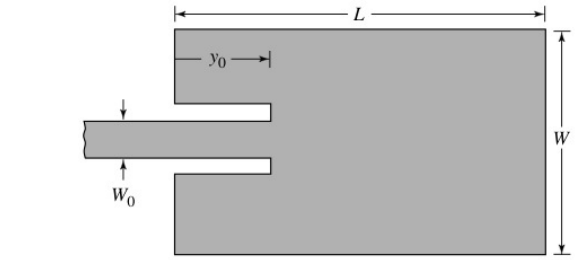

(a) Recessed microstrip-line feed

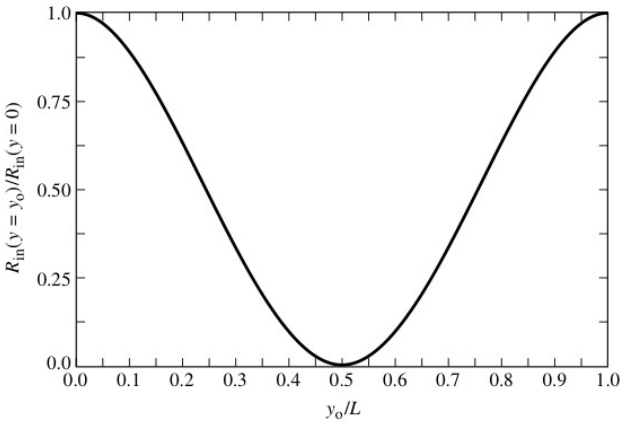

(b) Normalized input resistance

Figure 2.14: Recessed microstrip-line feed and variation of normalized input resistance [8].

Chapter 3

The Conformal Arrays

In this work various designs of conformal arrays were studied. As described in Chapter(2) a conformal array antenna consists of an array placed on a conformal surface, i.e. a surface that changes shape; consequently also the array changes shape. This can cause performance degradation: directivity and gain decrease while side lobe levels increase.

As described in Section(1.1.3), one of the most popular techniques adopted to mitigate the negative effects of array deformation is the projection method [18]. This method consists in the introduction of a proper phase-shift into the elements of the array in order to compensate for surface deformation. This phase-shift depends on various parameters like the geometry of the undeformed conformal array and its characteristics (direction of the main lobe, main lobe width, number of grating lobes, etc.), the shape of the deformation and the desired requirements for the deformed array. These parameters are different for each array design.

This chapter presents the features of the array systems implemented in this work: the requirements used for the design of the undeformed original linear array, the analyzed shape-deformation geometries and the

compensating phase-shifts for each of these geometries according to the projection method.

3.1 Linear Array

The starting point for the analysis of all the conformal array designs is an unbent linear array. This array consists of four or six patch antennas distanced of $\lambda/2$, placed on the xy plane (i.e. the ground of the patches lies in this plane) and aligned along the x-axis (Figure(3.1)). The distance among consecutive elements is computed as the distance among the phase-centers of the patch antennas.

The linear array made by four patch antennas is used as a reference for the study of the wedge, circular and S surface deformations, while the linear array made by six patches is used to study the Z deformation.

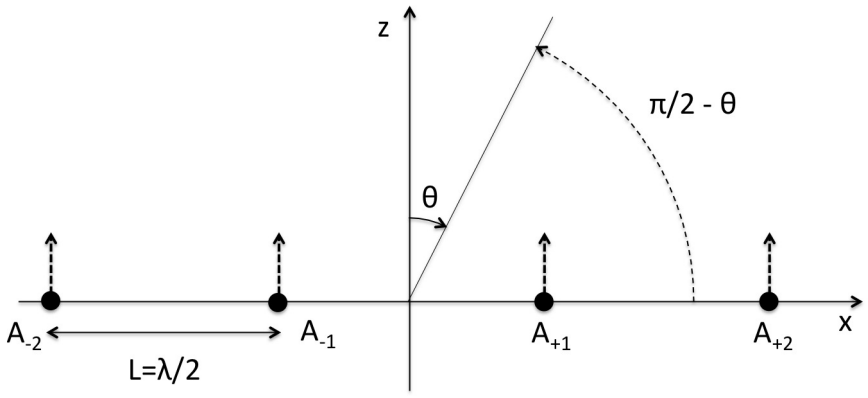

Figure 3.1: Model of the initial unbent 4-elements linear array.

The patch antenna that was used as the constituting element of the array was designed to resonate at $2.45GHz$, to have an input impedance of 50Ω and such that its dominant mode is q-TEM (quasi-TEM) (See Chapter(4) for the details of CST implementation). However, in order to apply the projection

method, the relevant information about the array is just its geometry, i.e. how the single elements are placed in space. Therefore, for this purpose, the single patch antennas are modeled as isotropic point sources, i.e. as antennas that irradiate homogeneously in every direction and whose dimensions in space are negligible.

Actually, this isn't the case for patch antennas since this type of antennas is not isotropic but instead directive: it shows a maximum in the $\vartheta = 0°$ direction (dashed arrow in Figure(3.1)). This fact has consequences when the array is deformed (as it will be shown in the next sections) since it affects the analytical calculation of the AF, as explained in section(1.1.3) and as shown by Eq.(1.29).

Nevertheless, when considering the original linear array, the information about the anisotropy of the patch is irrelevant. Infact in this case, all the patches have the same radiation pattern and this means that for the computation of the array characteristics, we can use the simplified formula for the AF (Eq.(1.12)):

$$AF = \left[\frac{\sin\left(\frac{N}{2}\psi\right)}{\sin\left(\frac{1}{2}\psi\right)}\right], \qquad \psi = kd\cos\left(\frac{\pi}{2} - \vartheta\right) + \beta \tag{3.1}$$

where the argument of the cosine is $\frac{\pi}{2} - \vartheta$ and not ϑ as in Eq.(1.12), because here a spherical coordinate system is adopted and so $\vartheta = 0°$ when the observation point is on the z-axis (while in Section(1.1.2) ϑ was $0°$ when the observation point was on the x-axis).

The chosen design, i.e. the distance between the elements set to $\lambda/2$ and a desired maximum required at $\vartheta = 0°$, leads to a phase-shift $\beta = 0$ between adjacent elements. Infact:

$$\frac{\psi}{2} = \frac{1}{2}\Big(kd\cos\Big(\frac{\pi}{2} - \vartheta\Big) + \beta\Big) = \frac{1}{2}\Big(\frac{2\pi}{\lambda} \cdot \frac{\lambda}{2}\cos\frac{\pi}{2} + \beta\Big) = \frac{\beta}{2} = 0 \qquad (3.2)$$

Therefore for the initial linear array, the required phase-shift between the elements is zero (when the array is deformed, this doesn't hold anymore). Moreover we can notice that, since the spacing between the elements is $\lambda/2 < \lambda$, there are no grating lobes (see Section(1.1.2)).

In order to evaluate the performance of the deformed arrays, their gains and directivities must be computed and compared with those of the original undeformed array. In order to do so, the multiplication pattern is used (see Chapter(2)) and the metrics for the linear array are evaluated: the total gain, directivity and electric-field are computed multiplying those of a single patch antenna by the AF given by:

$$AF = \sum_{n=1}^{N} w_n e^{j\psi_n} \qquad (3.3)$$

where $N = 4$ or $N = 6$, $w_n = a_n e^{j\delta_n} = ae^{j\delta}$ is the complex weight for element n and it comprises the amplitude and phase of the n-th exciting current [1] and ψ_n is given by:

$$\psi_n = kx_n \sin\vartheta \qquad (3.4)$$

where x_n is the x-ordinate of the n-th element and ϑ is the scan angle of the pattern.

[1] Since the array is uniform the amplitudes of the exciting currents are all equal, and since the required phase-shift between consecutive elements is 0, all the currents have equal phase components δ.

The analytical pattern of the linear arrays (with four or six elements) is used as a mean of comparison to evaluate the performance degradation of the deformed arrays and the effectiveness of the projection method as a pattern recovery technique.

3.2 Wedge Surface Deformation

When the surface on which the uniform array is placed, is bent of a concave angle ϑ_b, the array stops being linear and, as it will be shown in the next chapter, its performance deteriorate.

The first deformation-geometry that has been studied is represented in Figure(3.2) and consists of a wedge-shaped surface bent of an angle ϑ_b. As in the case of the linear array, the patch antennas are modeled as isotropic point sources and are labeled increasingly with respect to their x-ordinate, i.e. from left to right: $A_{-2}, A_{-1}, A_{+1}, A_{+2}$.

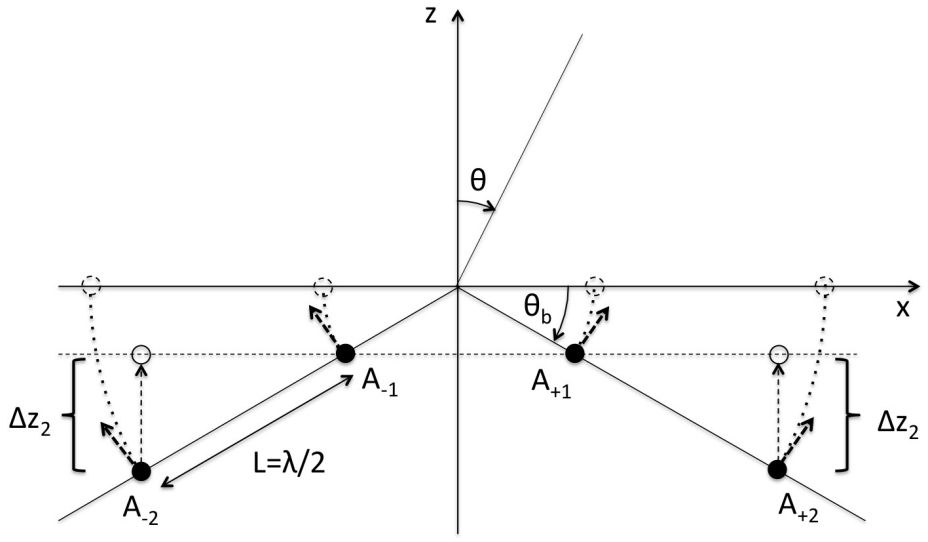

Figure 3.2: Wedge-shaped surface deformation of the original linear array.

In order to recover the radiation pattern of the deformed array, the projection method is applied. According to this, the first thing to do is project the elements of the deformed array onto a new reference plane. This is the plane perpendicular to the desired direction of maximum: in our case $\vartheta = 0°$, therefore the new reference plane will be parallel to the xy-plane. In particular, among the infinite planes with such characteristics, we choose it to be the nearest one to the elements of the array, i.e. the plane that comprises elements $A_{\pm 1}$ (dashed line in Fig.(3.2)).

The next step consists of computing the distance of the elements from their projections, i.e. Δz_n in Fig.(3.2):

$$\Delta z_{-2} = \Delta z_{+2} = \Delta z_2 = L \sin \vartheta_b \tag{3.5}$$

$$\Delta z_{-1} = \Delta z_{+1} = 0 \tag{3.6}$$

According to the projection method infact, the main cause of performance degradation lies in the fact that when the signals from elements $A_{\pm 2}$ arrive to the new reference plane, they are out-of-phase with respect to the signals emitted by elements $A_{\pm 1}$. This leads to the introduction of a phase-shift $\Delta\Phi$ with the purpose of compensating the difference in the distances traveled by the signals from $A_{\pm 2}$ to the new reference plane: $\Delta\Phi_2 = k \cdot \Delta z_2$ (and of course $\Delta\Phi_1 = 0$).

Analytically, after the introduction of the compensating phase-shift, the overall corrected AF of the deformed array becomes:

$$AF_{corrected} = AF_{wedge} \cdot e^{j\Delta\Phi} \tag{3.7}$$

In order to evaluate the overall radiation pattern of the array, the AF will be multiplied then for the radiation pattern of a single antenna.
Actually, as it was said in the previous section, this simplification applies when the single elements of the array are *isotropic* point-sources, so it holds for dipoles for examples, but not for patch antennas. Infact these antennas are directive and so we cannot apply the pattern multiplication rule (see 1.1) and simplify the overall radiation pattern as the product of the radiation of a single antenna by the AF given by (1.25):

$$AF = \sum_{n=-2}^{2} e^{jk[x_n(u-u_s)+y_n(v-v_s)+z_n\cos\vartheta]} \tag{3.8}$$

This is due to the fact that, in order to find the overall farfield of the array, we must scan the single antennas's pattern for each value of $\vartheta \in [-180°, 180°]$: if the antennas are isotropic, or even just parallel to the same plane, we can take the radiation pattern of a single antenna, and multiply it for the AF. While if the antennas's pattern are not isotropic nor parallel to the same plane, for each value of ϑ we must take the farfield of each antenna *in this direction*, multiply it by the term that takes into account the antenna's position (i.e. the AF in the simplified case of isotropic point sources), and finally sum all these terms together.
In order to illustrate this concept, in Fig.(3.2) the directions of the main lobes of each patch antenna are represented as dashed arrows.

Therefore the correct formula that must be used for the computation of the (*uncorrected*) analytical pattern is given by Eq(1.29):

$$AF = \sum_{n=-2}^{2} e(\vartheta - \vartheta_n) w_n e^{jk[x_n\sin\vartheta\cos\varphi+y_n\sin\vartheta\sin\varphi+z_n\cos\vartheta]} \tag{3.9}$$

where $e(\vartheta)$ is the radiation pattern of antenna n having a peak at $\vartheta = \vartheta_n$

and $e(\vartheta - \vartheta_n)$ is the pattern of the same element having instead a peak at $\vartheta = 0°$.

For simplicity's sake we will refer to this formula as another version of the AF, even if this is not precisely correct: this formula contains not only the contribution of the AF, but also the one of the radiation pattern of the single antenna $e(\vartheta - \vartheta_n)$.

In the case of a wedge-shaped surface bent of ϑ_b degrees, we have that the peak of the single patch antennas changes from $\vartheta = 0°$ when the array is unbent, to $\vartheta_{-2} = \vartheta_{-1} = -\vartheta_b$ and $\vartheta_{+2} = \vartheta_{+1} = \vartheta_b$ when the array si bent (see Fig.(3.2)). Thus the corrected analytical pattern of the array can be computed as:

$$AF = \sum_{n=-2}^{2} e(\vartheta - \vartheta_n) w_n e^{jk[x_n \sin\vartheta\cos\varphi + y_n \sin\vartheta\sin\varphi + z_n\cos\vartheta]} \cdot e^{j\Delta\Phi_n} \tag{3.10}$$

3.2.1 Reversed Wedge Surface Deformation

The second geometry that has been studied in this work is a variant of the wedge-shaped one described above: it is again wedge-shaped, but this time reversed, i.e. it's convex instead of concave as depicted in Figure(3.3).

The considerations made for the above-described geometry hold also for the reversed-one with just some differences. In this case, the new reference plane onto which the elements are projected is the one that comprises elements $A_{\pm 2}$, so the elements that must be projected onto this plane are elements $A_{\pm 1}$.

Therefore the roles of elements $A_{\pm 2}$ and $A_{\pm 1}$ are reversed. The phase-shift required for the elements of this array are given by:

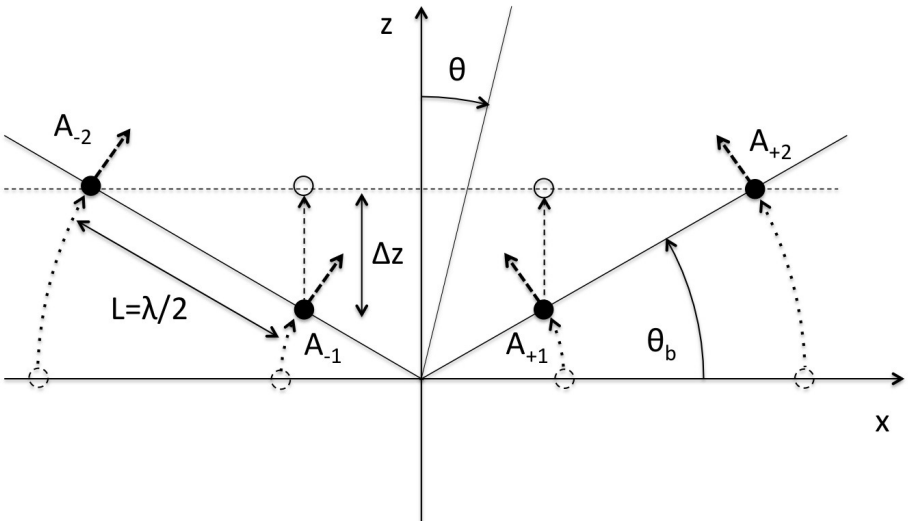

Figure 3.3: Convex wedge-shaped surface deformation of the original array.

$$\Delta z_{-1} = \Delta z_{+1} = \Delta z_1 = L \sin \vartheta_b \tag{3.11}$$

$$\Delta z_{-2} = \Delta z_{+2} = 0 \tag{3.12}$$

The formulas for the analytical pattern of the uncorrected and corrected cases are the same as those of the previous arrays (Eq.(3.9)-(3.7)), but this time with the new expressions for Δz_n.

Also in this case the directivity of the patch antennas must be taken into account as shown in Figure(3.3) for the computation of the overall radiation pattern: Eq.(3.9) applies but this time with $\vartheta_{-2} = \vartheta_{-1} = \vartheta_b$ and $\vartheta_{+2} = \vartheta_{+1} = -\vartheta_b$.

3.3 Z surface deformation

Another type of surface deformation that has been studied is the Z one given by the union of the concave and convex wedge deformations described in the previous section. In this case the original undeformed linear array consists of 6 patches distanced $\lambda/2$, instead of 4. This array is then doubly bent of an angle ϑ_b, resulting in a Z deformation as depicted in Figure(3.4).

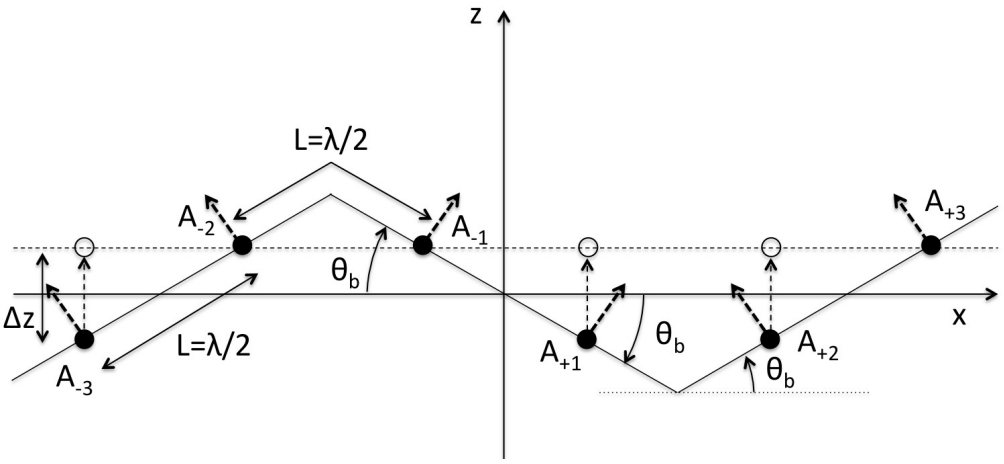

Figure 3.4: Z-shaped conformal array.

Also in this case the patch antennas are represented as isotropic point sources and they are numbered from left to right as A_{-3}, A_{-2}, A_{-1}, A_1, A_2, A_3.

Again, the projection method is applied in order to recover the radiation pattern of the deformed array. First, the new reference plane is chosen to be orthogonal to the main lobe direction, i.e. parallel to the xy-plane, and comprising elements A_{-2}, A_{-1}, A_3. Then elements A_{-3}, A_1, A_2 are projected onto the new reference plane and the distance between the elements and their projection is computed as $\Delta z = \Delta z_{-3} = \Delta z_1 = \Delta z_2 = L \sin \vartheta_b$ (and of course Δz is null for elements A_{-2}, A_{-1}, A_3).

At this point the compensating phase-shifts for the projected elements can be computed as:

$$\Delta\Phi = \Delta\Phi_{-3} = \Delta\Phi_1 = \Delta\Phi_2 = k\Delta z \tag{3.13}$$

Also for this type of surface deformation the patch antennas don't have all the same radiation pattern since they are inclined of an angle $\pm\vartheta_b$. Therefore, in order to compute the analytical overall (*uncorrected*) radiation pattern of the array, this information must be taken into account and Eq.(3.9) must be used:

$$AF = \sum_{n=-3}^{3} e(\vartheta - \vartheta_n) w_n e^{jk[x_n \sin\vartheta\cos\varphi + y_n \sin\vartheta\sin\varphi + z_n\cos\vartheta]}$$

where again $w_n = a_n e^{j\delta n} = a e^{j\delta}$, $e(\vartheta)$ is the radiation pattern of antenna n having a peak at $\vartheta = \vartheta_n$ and $e(\vartheta - \vartheta_n)$ is the pattern of the same element having instead a peak at $\vartheta = 0°$.
In this case we have that: $\vartheta_{-3} = \vartheta_{-2} = \vartheta_2 = \vartheta_3 = -\vartheta_b$ while $\vartheta_{-1} = \vartheta_1 = \vartheta_b$.

Finally the corrected analytical pattern can be computed using Eq.(3.10):

$$AF = \sum_{n=-3}^{3} e(\vartheta - \vartheta_n) w_n e^{jk[x_n \sin\vartheta\cos\varphi + y_n \sin\vartheta\sin\varphi + z_n\cos\vartheta]} \cdot e^{j\Delta\Phi_n}$$

3.4 Circular Surface Deformation

The other conformal array studied in this work, consists of a 4-elements linear array bent on a concave arc of circumference of radius r, as depicted in Figure(3.5).

Again the elements are modeled as isotropic point sources and they are

numbered in an identical manner as in the previous case: from left to right $A_{-2}, A_{-1}, A_{+1}, A_{+2}$.

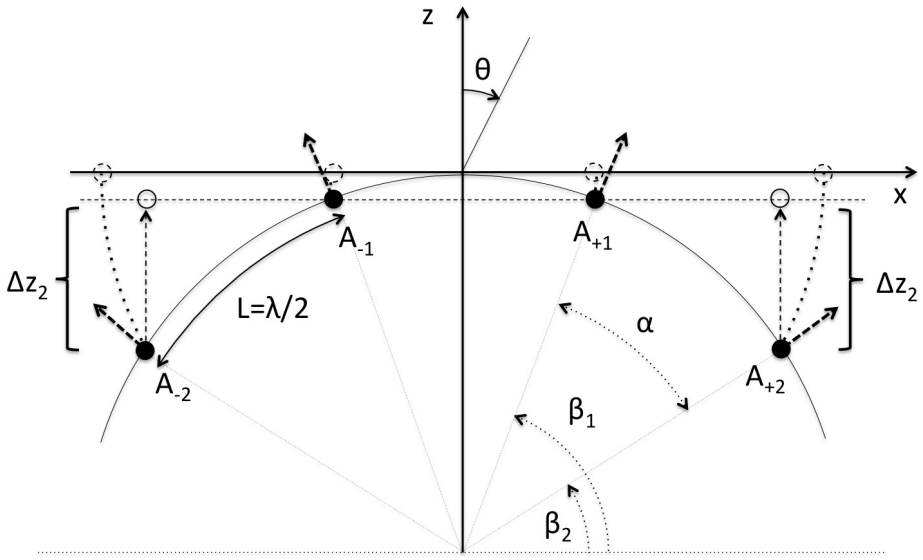

Figure 3.5: Conformal array on a concave circular surface.

As in the previous cases, the projection method is adopted in order to recover the radiation pattern of the deformed array.

Again first of all, the new reference plane is defined as the plane orthogonal to the desired direction of maximum, i.e. as the plane parallel to the xy plane, in particular, it is chosen to be the one that comprises elements $A_{\pm 1}$.

Then elements $A_{\pm 2}$ are projected onto the new reference plane and their distances from their projections are evaluated. In order to do so, the coordinates of the elements are identified. Referring to Fig.(3.5), the angle α is computed in radians as $\alpha = \frac{L}{r} = \frac{\lambda/2}{r}$.
Consequently we can get β_1 and β_2 as: $\beta_2 = \frac{\pi - 3\alpha}{2}$ and $\beta_1 = \beta_2 + \alpha$.

Thus, the coordinates of the elements are given by:

$$A_{-2}: \quad (-r\cos\beta_2, 0, -(r - r\sin\beta_2)) \tag{3.14}$$

$$A_{-1}: \quad (-r\cos\beta_1, 0, -(r - r\sin\beta_1)) \tag{3.15}$$

$$A_{+1}: \quad (r\cos\beta_1, 0, -(r - r\sin\beta_1)) \tag{3.16}$$

$$A_{+2}: \quad (r\cos\beta_2, 0, -(r - r\sin\beta_2)) \tag{3.17}$$

and this implies that: $\Delta z = \Delta z_2 = \Delta z_{-2} = z_{\pm 1} - z_{\pm 2} = r(\sin\beta_1 - \sin\beta_2)$.

So the phase-shift that must be introduced in elements $A_{\pm 2}$ is given by $\Delta\Phi = k\Delta z$. Analogous considerations as those of the previous section hold for the analytical computation of the AF: since the single elements are again patch antennas and so directive antennas, the overall *corrected* pattern must be computed using Eq.(3.10) as:

$$AF = \sum_{n=-2}^{2} e(\vartheta - \vartheta_n) w_n e^{jk[x_n \sin\vartheta\cos\varphi + y_n \sin\vartheta\sin\varphi + z_n\cos\vartheta]} \cdot e^{j\Delta\Phi_n}$$

where again ϑ_n is the maximum direction of element n, that this time is equal to:

$$\vartheta_{-2} = -\beta_2\ , \qquad \vartheta_{+2} = \beta_2$$
$$\vartheta_{-1} = -\beta_1\ , \qquad \vartheta_{+1} = \beta_1$$

3.4.1 Reversed Circular Deformation Surface

A variant of the circular surface deformation is the convex one, depicted in Figure(3.6). For this type fo conformal arrays, similar considerations to the

ones just exposed hold. The numbering and modeling of the single antennas is the same, the reference plane is again parallel to the xy-plane but this time it's the one comprising elements $A_{\pm 2}$, so $A_{\pm 1}$ are the elements that have to be projected onto the new reference plane and to which a correcting phase-shift must be applied.

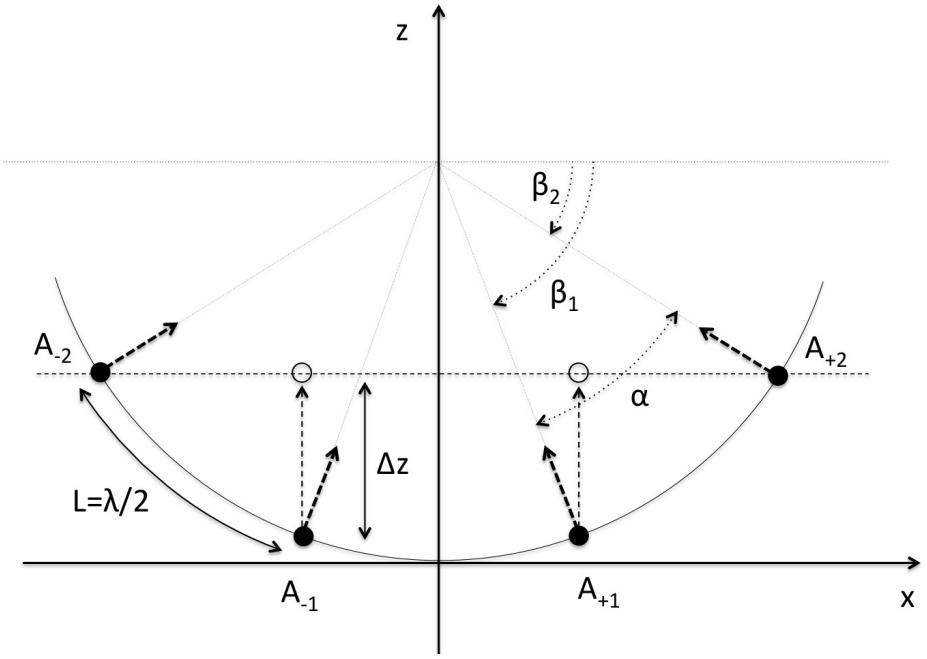

Figure 3.6: Conformal array on a convex circular surface.

Again, in order to apply the projection method, the distance between elements $A_{\pm 1}$ and their projections must be evaluated. For this purpose, first the coordinates of the elements must be computed:

$$A_{-2}: \quad (-r\cos\beta_2, 0, (r - r\sin\beta_2)) \tag{3.18}$$

$$A_{-1}: \quad (-r\cos\beta_1, 0, (r - r\sin\beta_1)) \tag{3.19}$$

$$A_{+1}: \quad (r\cos\beta_1, 0, (r - r\sin\beta_1)) \tag{3.20}$$

$$A_{+2}: \quad (r\cos\beta_2, 0, (r - r\sin\beta_2)) \tag{3.21}$$

where angles α and $\beta_{1,2}$ are the same as in the previous case. So the distance of elements $A_{\pm 1}$ from the reference plane is $\Delta z = \Delta z_{-2} = \Delta z_2 = z_{\pm 2} - z_{\pm 1} = r(\sin\beta_1 - \sin\beta_2)$, and the required phase-shift is $\Delta\Phi = \Delta\Phi_{-1} = \Delta\Phi_1 = k \cdot \Delta z$.

As for the previous conformal geometries, the directivity of the patch antennas must be taken into account when evaluating the overall corrected analytical pattern of the array as:

$$AF = \sum_{n=-2}^{2} e(\vartheta - \vartheta_n) w_n e^{jk[x_n \sin\vartheta\cos\varphi + y_n \sin\vartheta\sin\varphi + z_n\cos\vartheta]} \cdot e^{j\Delta\Phi_n}$$

where the directions of maximum for the elements of this conformal arrays are given by:

$$\vartheta_{-2} = \beta_2\ , \qquad \vartheta_{+2} = -\beta_2$$

$$\vartheta_{-1} = \beta_1\ , \qquad \vartheta_{+1} = -\beta_1$$

3.5 S surface deformation

The last conformal array that has been studied in this work consists of a 4-elements linear array bent on an S-shaped surface as depicted in Figure(3.8). In order to apply the projection method and therefore to derive the compensating phase-shifts to be introduced in each array's element, it is useful to understand how this surface deformation has been obtained starting from the uniform linear array described in Section(3.1).

As a first step, the linear array was bent on a surface that is the union of the two arcs of circumference described in the previous section: the left part of the array was bent following the convex arc of circumference, while the second one was bent following the concave one as depicted in Fig.(3.7).

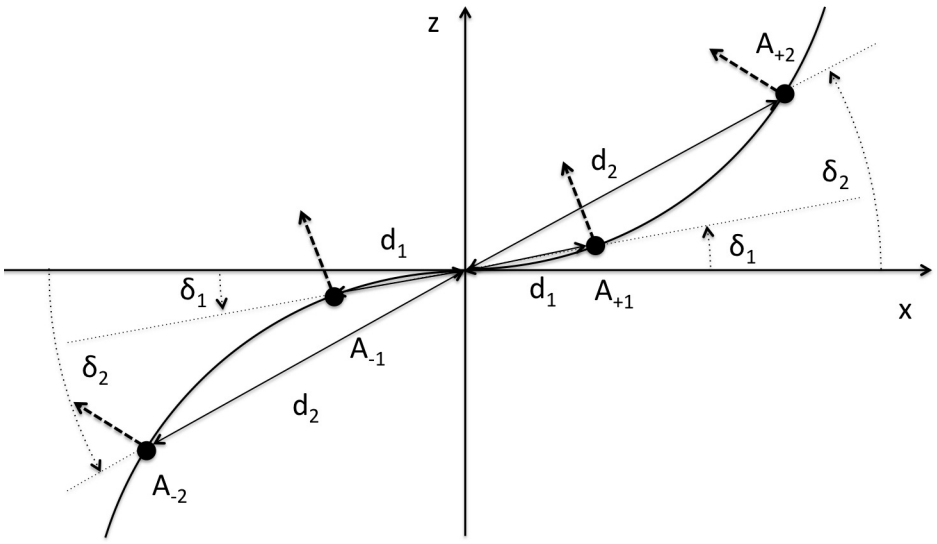

Figure 3.7: S-shaped unrotated conformal array.

The elements are numbered and modeled as in the previous cases and their coordinates at this point of the bending process are given by (3.14)-(3.15)-(3.21)-(3.20) for elements A_{-2}, A_{-1}, A_1, A_2 rispectively:

$$A_{-2}: \quad (x^0_{-2}, 0, z^0_{-2}) = (-r\cos\beta_2, 0, -(r - r\sin\beta_2)) \tag{3.22}$$

$$A_{-1}: \quad (x^0_{-1}, 0, z^0_{-1}) = (-r\cos\beta_1, 0, -(r - r\sin\beta_1)) \tag{3.23}$$

$$A_{+1}: \quad (x^0_{1}, 0, z^0_{1}) = (r\cos\beta_1, 0, (r - r\sin\beta_1)) \tag{3.24}$$

$$A_{+2}: \quad (x^0_{2}, 0, z^0_{2}) = (r\cos\beta_2, 0, (r - r\sin\beta_2)) \tag{3.25}$$

where the values of the angles are again given by:

$$\alpha = \frac{L}{r} \qquad \beta_2 = \frac{\pi - 3\alpha}{2} \qquad \beta_1 = \beta_2 + \alpha \tag{3.26}$$

After this, the obtained array was clock-wise rotated of an angle α, thus obtaining the final configuration of the array (solid line in Fig.(3.8)).

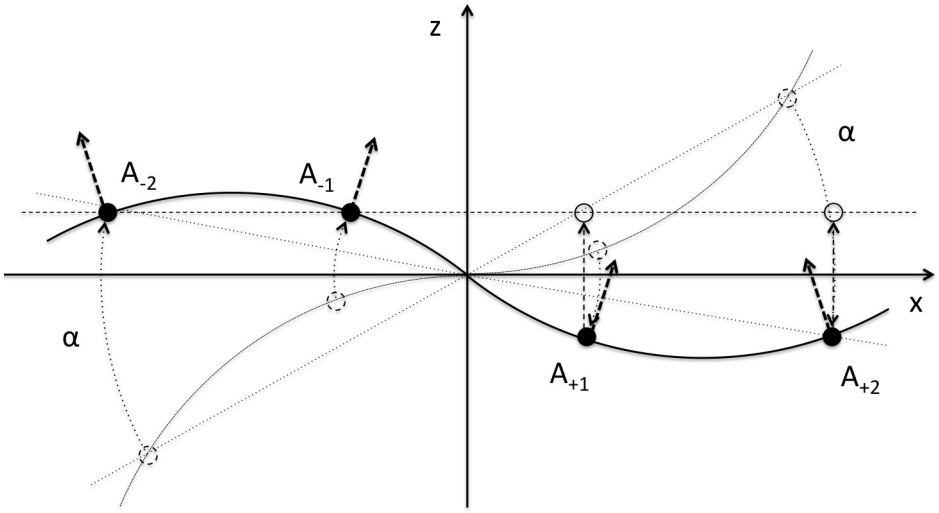

Figure 3.8: S-shaped rotated conformal array.

Before applying the projection method to this configuration, it's necessary to derive the ultimate elements's coordinates. In order to do so, we can define the angles formed by the x-axis and the segment connecting the elements to

the axis's origin (see Fig.(3.8)):

$$\delta_2 = \arctan\left|\frac{z^0_{-2}}{x^0_{-2}}\right| = \arctan\left|\frac{z^0_2}{x^0_2}\right| \tag{3.27}$$

$$\delta_1 = \arctan\left|\frac{z^0_{-1}}{x^0_{-1}}\right| = \arctan\left|\frac{z^0_1}{x^0_1}\right| \tag{3.28}$$

and the length of the above-mentioned segments:

$$d_2 = \sqrt{(x^0_{-2})^2 + (z^0_{-2})^2} = \sqrt{(x^0_2)^2 + (z^0_2)^2} \tag{3.29}$$

$$d_1 = \sqrt{(x^0_{-1})^2 + (z^0_{-1})^2} = \sqrt{(x^0_1)^2 + (z^0_1)^2} \tag{3.30}$$

Thus, the elements's coordinates become:

$$A_{-2}: \quad (x_{-2}, 0, z_{-2}) = (-d_2\cos(\alpha - \delta_2), 0, d_2\sin(|\alpha - \delta_2|)) \tag{3.31}$$

$$A_{-1}: \quad (x_{-1}, 0, z_{-1}) = (-d_1\cos(\alpha - \delta_1), 0, d_1\sin(|\alpha - \delta_1|)) \tag{3.32}$$

$$A_{+1}: \quad (x_1, 0, z_1) = (d_1\cos(\alpha - \delta_1), 0, -d_1\sin(|\alpha - \delta_1|)) \tag{3.33}$$

$$A_{+2}: \quad (x_2, 0, z_2) = (d_2\cos(\alpha - \delta_2), 0, -d_2\sin(|\alpha - \delta_2|)) \tag{3.34}$$

And in this way elements A_{-2}, A_{-1} lie on a line parallel to the x-axis, as well as elements A_1, A_2 lie on another line parallel to the x-axis.

The last information needed in order to apply the projection method is the direction of maximum of each of the four patch antennas (dashed arrows in Fig.(3.7)-(3.8)), so that their directivity can be taken into account in the analytical evaluation of the overall radiation pattern. After the array is bent

along the S surface but before it is rotated of α degrees, the direction of maximum are given by:

$$\vartheta^0_{-2} = \vartheta^0_2 = -\beta_2 \qquad \vartheta^0_{-1} = \vartheta^0_1 = -\beta_1 \tag{3.35}$$

while after the array is rotated of α degrees, they become:

$$\vartheta_{-2} = \vartheta_2 = -\beta_2 + \alpha \qquad \vartheta_{-1} = \vartheta_1 = -\beta_1 + \alpha \tag{3.36}$$

At this point the projection method can be applied: the new reference plane is parallel to the x-axis and it passes through elements A_{-2}, A_{-1}. The distance of elements A_1, A_2 from this plane can be computed as: $\Delta z = \Delta z_1 = \Delta z_2 = z_{-1} - z_1 = 2d_1 \sin(|\alpha - \delta_1|)$. Therefore the compensating phase-shift that must be introduced in elements A_1, A_2 is $\Delta\Phi = k \cdot \Delta z$, and the overall corrected analytical radiation pattern is given again by Eq.(3.10):

$$AF = \sum_{n=-2}^{2} e(\vartheta - \vartheta_n) w_n e^{jk[x_n \sin\vartheta\cos\varphi + y_n \sin\vartheta\sin\varphi + z_n\cos\vartheta]} \cdot e^{j\Delta\Phi_n}$$

where ϑ_n are given by (3.36).

At this point the models for all the conformal arrays studied in this work have been presented. The next chapter describes the implementation of the different systems in CST and MATLAB and presents the obtained numerical results.

Chapter 4

Implementation and Results

The different conformal arrays described in Chapter(1) have been implemented and studied with the support of two software programs: matlab and "CST Microwave Studio". Part of this project was also developed in collaboration with the North Dakota State University of Fargo, North Dakota (US) that realized the prototypes of some of the conformal arrays presented in this work.

This chapter is devoted to the description of the matlab and CST implementation of the various conformal arrays, and to the discussion of the results obtained applying the projection method as a pattern-recovery technique.

First of all, the single patch's CST implementation is presented, then the 4-elements linear array is considered together with all the studied deformation of this array: circular, circular reversed, S-shaped, wedge 30°, wedge 30° reversed, wedge 45°. Finally the 6-elements linear array is considered together with its Z-shaped deformation.

4.1 Single Patch Antenna

All the conformal arrays that have been studied in this work have been designed using the same single-element antenna: a patch antenna resonating at $2.45\,GHz$ and with an input impedance of $50\,\Omega$. In order to correctly implement the patch antenna using CST Microwave Studio, the design rules presented in Chapter(1.2) were applied as a first step.

Referring to Figure(4.1), given the height of the substrate and the substrate material, the width W and length L of the patch were determined in such a way that the desired resonant frequency is matched by the patch.

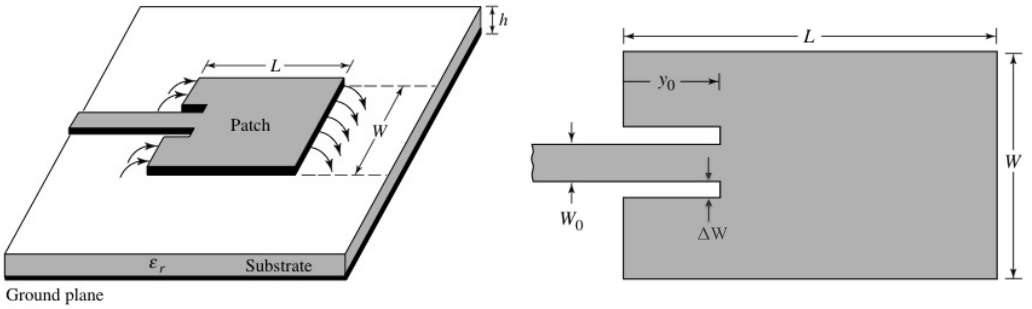

Figure 4.1: Patch antenna representation with its characteristics dimensions.

The substrate is made of Arlon CLTE lossy that is characterized by a relative dielectric constant $\varepsilon_r = 2.94$, a relative permeability $\mu = 1$ and a loss tangent $\tan\delta = 0.0025$. With this knowledge a first estimate of W and L was possible: these values were then optimized in CST in order to get a sufficiently low value for the reflection parameter S_{11} at the desired frequency $f = 2.45\,GHZ$. Moreover the patch and the ground were modeled as infinitely thin sheets in CST.

As far as W_0 and y_0 are concerned, they have been chosen in such a way that the input impedance of the antenna is 50Ω and that the fundamental mode that propagates is q-TEM.

Table(4.1) reports the final values of the parameters depicted in Fig.(4.1).

Parameter	Value $[mm]$
h	1.52
W	43.70
L	35.33
W_0	4.1
y_0	11
ΔW	1.94

Table 4.1: Patch parameters values.

In order to simulate the patch antenna in CST, the frequency solver was used and the simulation frequency range was chosen to be $f \in [2.2,\, 2.7]\, GHz$. A discrete port with input impedance $Z = 50\Omega$ was used together with a tetrahedral mesh and the enablement of the adaptive mesh refinement option in order to get better accuracy.

Figure (4.2a) reports the 3-dimensional electric farfield of the antenna, while Fig.(4.2b) reports the polar plot of the gain measured for $\varphi = 0°$ and varying ϑ. It can be seen how the patch antenna is directive and in particular that it shows a maximum for $\vartheta = 0°$ of $5.78\, dB$ and that the angular half-power width[1] of the main lobe is 88°.

Finally Figure(4.3) reports the patch's S_{11} parameter: it's evident how the resonant frequency can be considered $2.45\, GHz$.

4.2 Four-Elements Linear Array

In order to increase the directivity of the single patch, i.e. in to reduce the angular width of the main lobe of Fig.(4.2b), four patch antennas were then aligned along the x-axis in order to form a linear array. This is the array

[1] i.e. the angular main lobe beamwidth, that is defined as the angle between the half-power points of the main lobe, i.e. the angle between the lightblue lines in Fig.(4.2b).

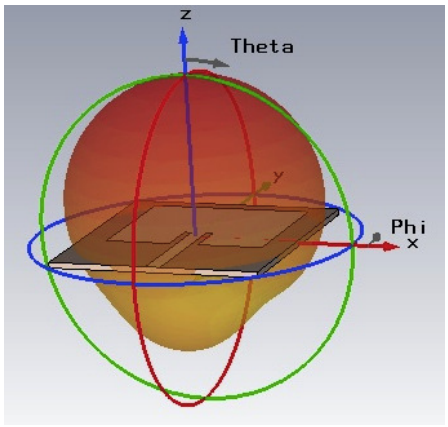

(a) 3D Farfield of a patch.

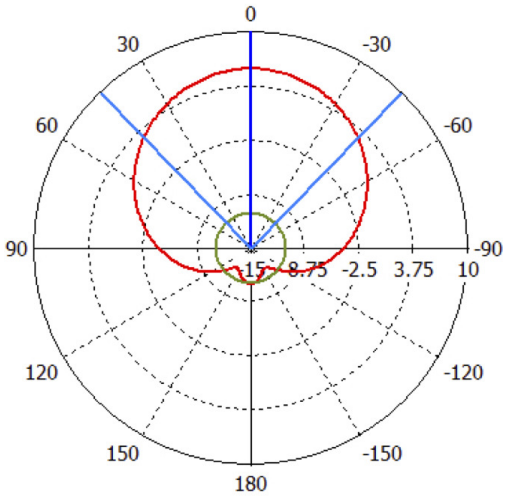

Frequency = 2.45
Main lobe magnitude = 5.78 dB
Main lobe direction = 0.0 deg.
Angular width (3 dB) = 88.0 deg.
Side lobe level = -16.7 dB

(b) Farfield Gain of a patch.

Figure 4.2: Single patch's radiation pattern: 3D farfield and polar gain.

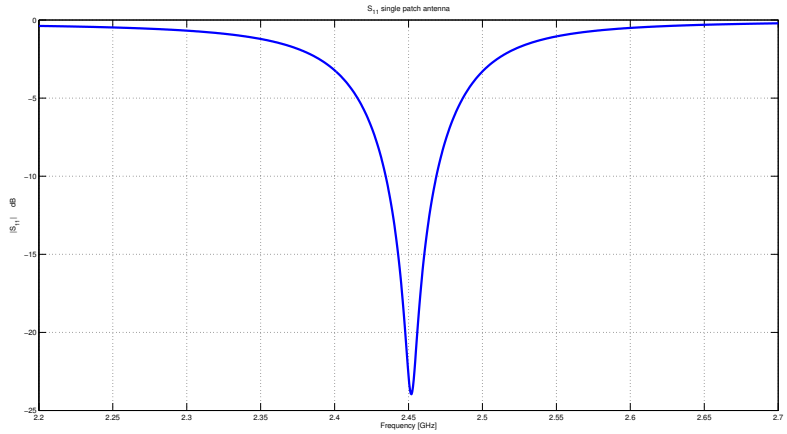

Figure 4.3: S_{11}.

that has been deformed according to various surface's geometries, therefore it is important to characterize it so that a comparison for the performance of the conformal arrays is available.

As a first thing, the analytical pattern of the array's electric field was obtained in matlab exploiting the theoretical concepts exposed in Chapter(1): the superposition of effects principle was used multiplying the radiation pattern of the single patch antenna (red plot in Fig.(4.4)) with the AF. This pattern was then compared with the one obtained through CST simulation and a good match between these two can be noticed (green and black line respectively in Fig.(4.4)) thus validating the CST model and showing that the effects of mutual coupling among the antennas is in this case negligible: infact the main difference between the theoretical matlab implementation and the CST simulation of the array resides in the absence/presence of mutual coupling among the elements respectively.

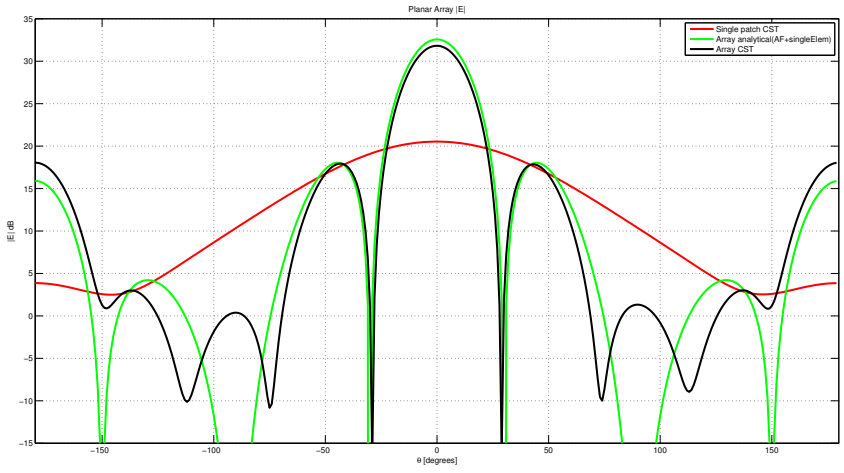

Figure 4.4: Electric Field of a 4-elements linear array.

If the radiation pattern of the array is compared with the one of the single patch antenna, it can be noticed that the gain is increased approximately of

a factor of 4 (in linear scale), while the 3-dB main lobe width decreases approximately of the same factor: from 88° to 24.6°. This can be seen by comparison of Figure(4.5), that represents the gain pattern for the linear array, with Fig(4.2b).

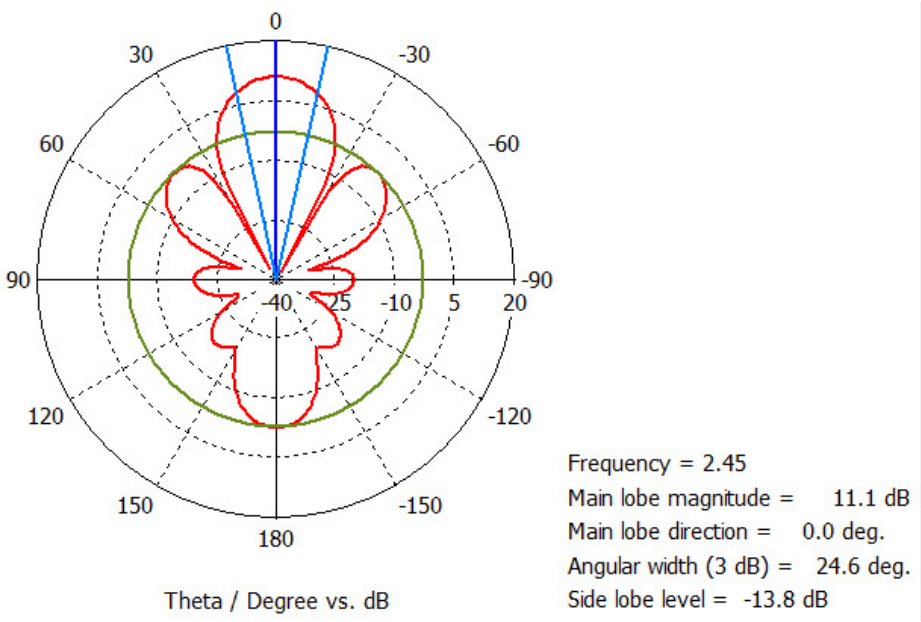

Figure 4.5: Gain's polar plot of the 4-elements linear array.

4.3 Circular Conformal Array

When the linear array is bent on a circular conformal surface (in this particular case the radius of the surface is $r = 10\,cm$), as represented in Figure(4.6) the obtained radiation pattern is different from the one of the linear array.

In matlab the theoretical pattern of the electric farfield was obtained implementing Eq.(1.10):

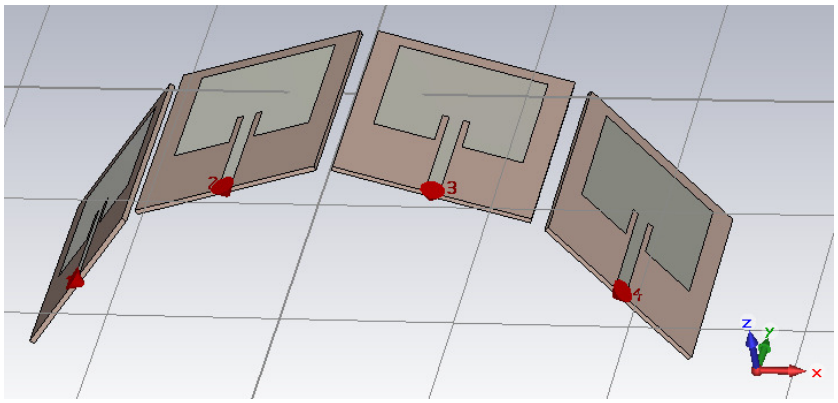

Figure 4.6: CST design of the circular conformal array.

$$AF = \sum_{n=-2}^{2} e(\vartheta - \vartheta_n) w_n e^{jk[x_n \sin\vartheta\cos\varphi + y_n \sin\vartheta\sin\varphi + z_n\cos\vartheta]} \cdot e^{j\Delta\Phi_n}$$

where the meaning of all the terms is explained in Section(1.4) and where the single element's electric field $e(\vartheta - \vartheta_n)$ is the electric field of the patch antenna described above with a maximum in correspondence of 0° (red line in Fig.(4.4)).

The CST implementation of the system is straightforward: starting from a single patch antenna, this antenna was copied and moved in the four points of the circular line described in Section(1.4) (see Fig.(1.5)); finally each patch antenna was rotated in order to be tangent to the circular surface. All the other settings (simulation frequency range, type of solver and mesh, etc.) are identical to those of the previous cases (they are the same for all the studied conformal arrays).

As it was explained in Chapter(1) when the array is bent its performance degrades: the main lobe direction can change, main lobe gain decreases while angular width increases. This is exactly what happens for this conformal

array.

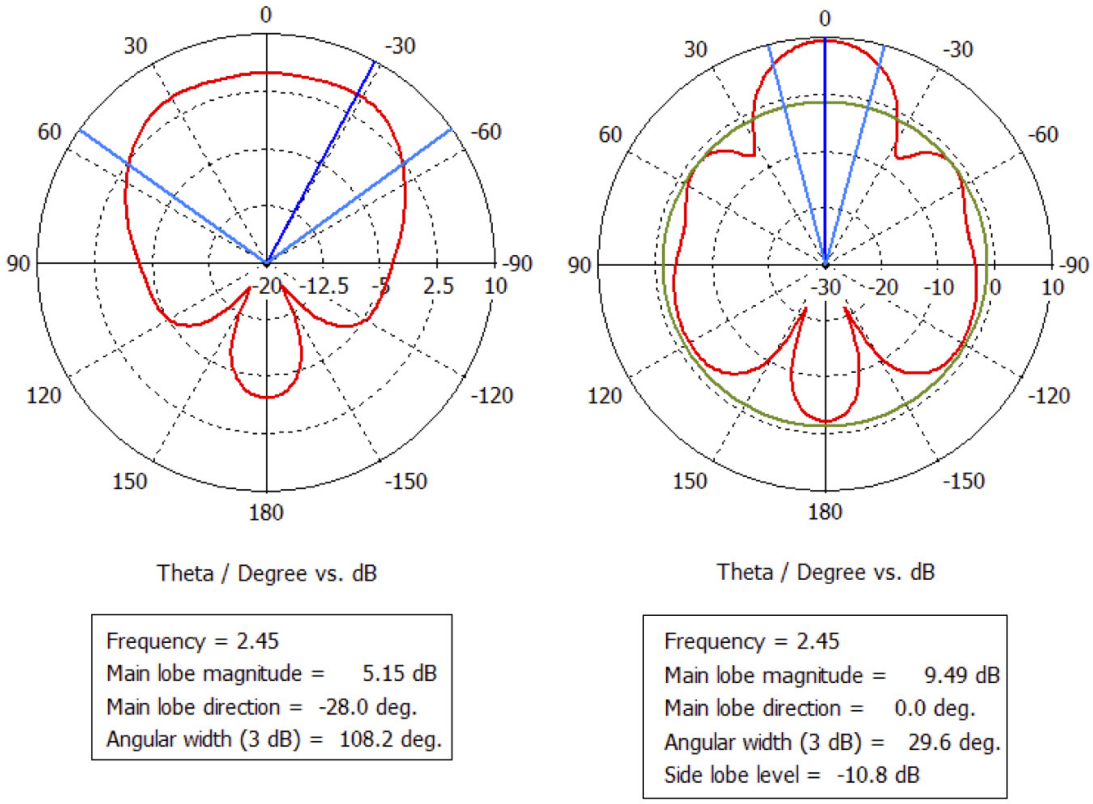

Figure 4.7: Gain's polar plot of the circular array: uncorrected (left) and corrected (right).

Fig(4.7) on the left represents the gain of the array when no pattern-recovery technique is adopted: it can be seen how the main lobe direction has changed from $0°$ to $-28°$ and how the angular width is $108.2°$ that is much greater than the one of the linear array and even than the one of the single patch. Moreover the gain in the main lobe direction is $5.15\,dB$ that is lower than both the one of the linear array and the single patch. Therefore we can conclude that performance has degraded.

If the projection method is applied in order to recover the radiation pattern of the array, i.e. if a proper phase-shift is introduced in the first

and last elements (see Section(1.4)), the performance of the array improves. The array's gain after the introduction of the compensating phase-shift is reported in the right-most part of Fig.(4.7): the main lobe direction moves back to 0°, the gain in this direction increases of more of more than a factor 2.5 (in linear scale) becoming $9.49\,dB$ and approaching the $11.1\,dB$ of the linear array; moreover also the angular width of the main lobe decreases of a factor higher than 3.5 passing from 108.2° to 29.6° almost reaching the 24.6° of the linear array.

Figure(4.8) shows also that there is good agreement between matlab and CST simulations: the blue line is the analytical electric field obtained by matlab simulation, while the black line is the E-field obtained by CST simulation.

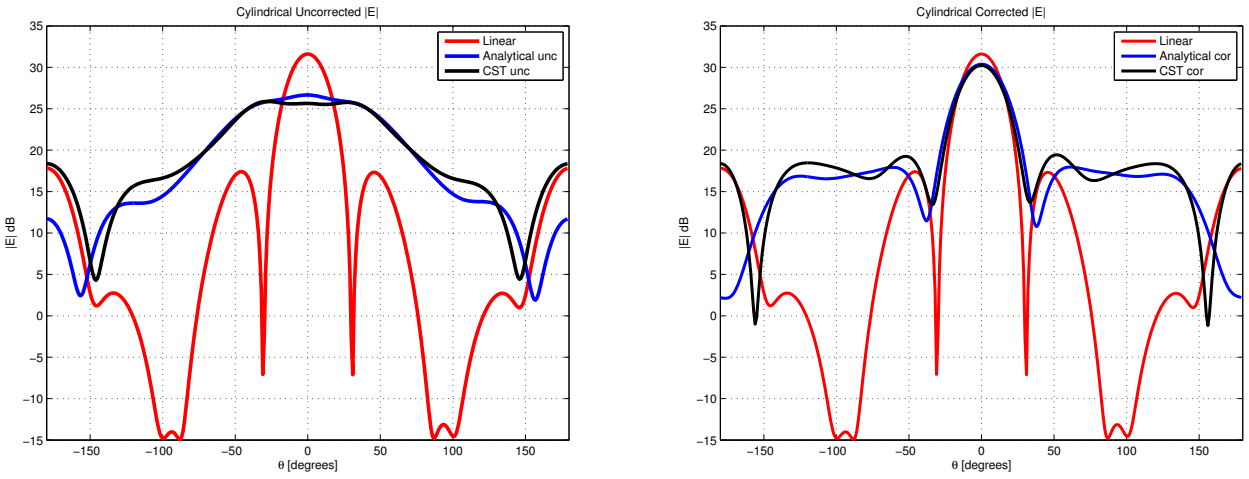

(a) Uncorrected.

(b) Corrected.

Figure 4.8: Circular conformal array E-field: Analytical (blue), simulated (black) and desired, i.e. linear array (red) patterns.

The two Figures(4.8) show the electric farfield with and without compensating phase-shift, in comparison with the desired pattern of the

linear array: applying the projection method the pattern is partially recovered, especially in the main lobe direction, but from 90° to 180° the pattern can't be recovered in an equally effective way.

Figure(4.9) represents the synthesis of the study on this conformal array: its CST-simulated uncorrected E-pattern, the corrected one and the desired ideal one, i.e. that of the linear array.

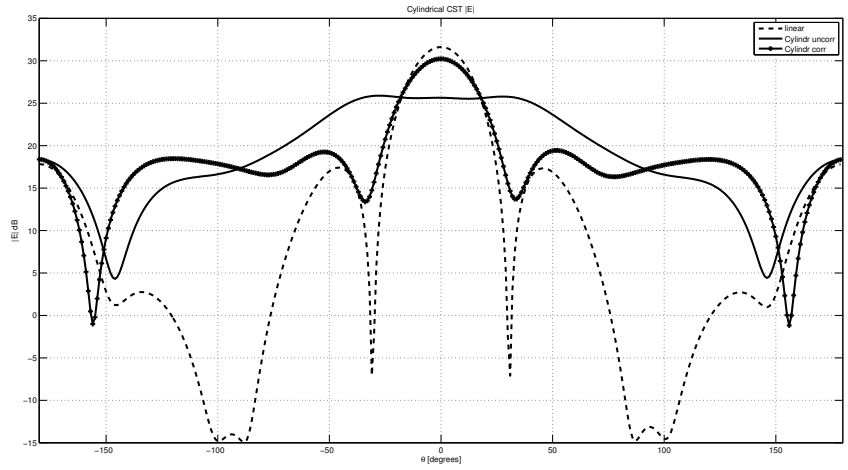

Figure 4.9: Circular array: CST-simulated E-field. Linear array (dashed line), circular uncorrected (plain) and corrected (marked).

Therefore we can conclude that the projection method works fine as a pattern recovery technique but it also shows some limitations: it enables pattern recovery in the main lobe direction but its recovery capability decreases as soon as directions distant from broadside are considered. This fact can be regarded as the price to be paid for the tradeoff between implementation simplicity and recovery capability: other more complex pattern-recovery techniques could be used resulting in better improvements, but at the expense of more complex control-systems.

The prototype of this conformal array was realized and characterized by researchers of the North Dakota State University, Fargo, ND, USA: Fig.(4.12) reports the analytical results (obtained by HFSS simulations) together with the measured ones. It can be seen how there is good correspondence between the measurements and the analytical results; moreover it can be seen how these results match the ones obtained in this work[2].

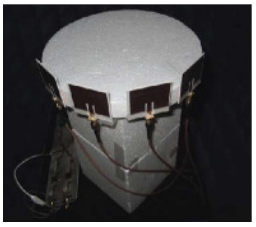

Figure 4.10: Prototype.

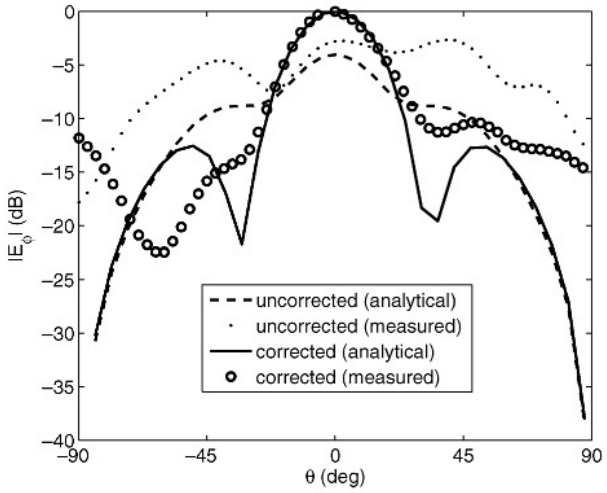

Figure 4.11: Relative E-field.

Figure 4.12: Prototype and numerical results (analytical and measured) of the circular conformal array obtained in [19] at the North Dakota State University, Fargo, ND, USA.

4.3.1 Reversed Circular Conformal Array

Another conformal array that has been studied is the one obtained adapting the linear array on a reversed circular surface as depicted in Fig.(4.13). This

[2]This fact can be seen comparing Figures(4.12) and (4.9) and considering that in the first one ϑ is limited in the range $[-90°, 90°]$ (instead of the full range $[-180°, 180°]$ of Fig.(4.9)) and that the E-field is depicted in a relative scale, i.e. the maximum is assumed to be $0\,dB$ (while in the other case the maximum is the farfield value of the electric field expressed in dBV/m).

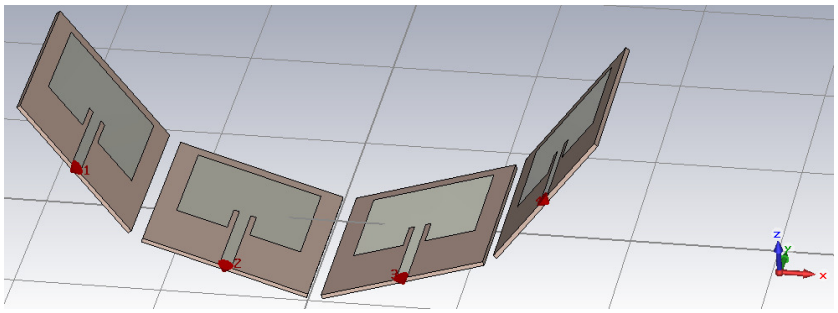

Figure 4.13: CST design of the concave circular conformal array.

array is very similar to the one described above, therefore similar results and considerations can be made for this configuration: the matlab and CST implementation derive immediately from what was said about the previous conformal array.

Also in this case, when the array is bent its performance downgrades. Fig(4.14) on the left represents the gain of the array when no pattern-recovery technique is adopted: it can be seen how the angular width is 108.6° that is much greater than the one of the linear array and even than the one of the single patch. Moreover the gain in the main lobe direction is $5.74\,dB$ that is lower than both the one of the linear array and the single patch.

These results are very similar to the previous case, even if in this case things are slightly better since at least the main lobe direction remains at 0° [3].

Applying the projection method, i.e. introducing a proper phase-shift in the two elements in the middle of the array (see Section(1.4)), the performance of the array improves. The array's gain after the introduction of the compensating phase-shift is reported in the right-most part of Fig.(4.14): the gain in the maximum direction doubles (in linear scale) becoming $8.88\,dB$

[3]Actually in the previous case, the maximum of $5.15\,dB$ occured at $-28°$, but at 0° the gain was $5\,dB$, so there is no big difference between the gain value in the maximum direction and at broadside.

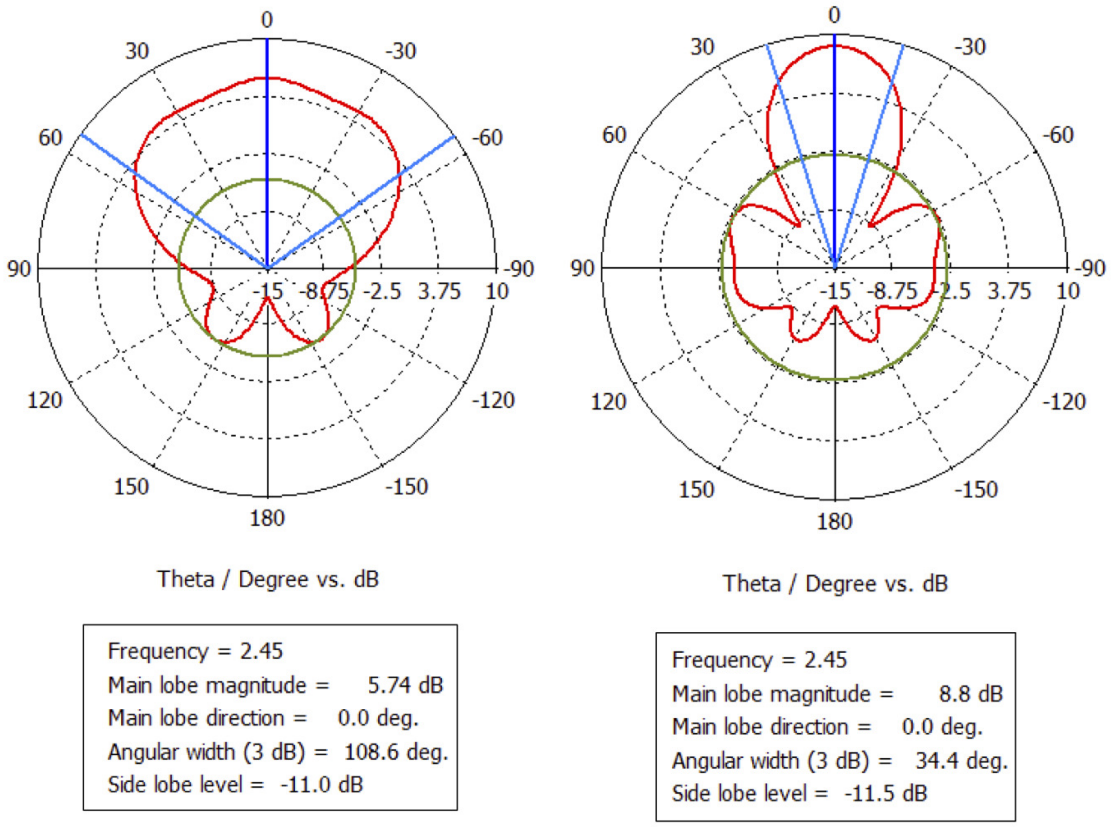

Figure 4.14: Polar plot of the array gain for the uncorrected (left) and corrected (right) cases (rev. circular array).

and approaching the 11.1 dB of the linear array; moreover also the angular width of the main lobe decreases of a factor 3 passing from 108.6° to 34.4°.

The correcting capability of the projection method is slightly worse in this case with respect to the previous one: the gain increases of a factor 2 instead of 2.5 and it reaches 8.88 dB instead of the 9.49 dB of the previous case. Also the recovered angular width in this case is greater than in the previous case (34.4° vs 29.6°).

Appearently this discrepance isn't justified, since the relative distances among the projections of the array elements onto the x-axis are the same in both cases (both lower than $\lambda/2$). But there is a difference between the

two conformal arrays: in the previous case, each patch antenna radiated with a maximum direction divergent from broadside, while in this case the maxima of the antennas are converging towards broadside and therefore they are pointing towards the other antennas's radiating slots (i.e. towards the antennas's patches). This implies a higher degree of mutual coupling with respect to the concave array as it can be seen inspecting the values of the parameters S_{21}, S_{32}, S_{43} at $2.45\,GHz$ in the two cases:

Circular Array	S_{21} $[dB]$	S_{32} $[dB]$	S_{43} $[dB]$
Concave	-20	-24	-20
Convex	-12	-14	-12

it's evident how changing the conformal surface from concave to convex implies an increase in these S parameters of almost $10\,dB$ that denotes a higher level of mutual coupling. As far as the convex array is concerned, all these S parameter values are higher than $-15\,dB$, so that mutual coupling has an impact on the performance of the array and therefore also on the performance of the projection method, thus explaining the different effectiveness of this pattern recovery technique in the two cases.

Figure(4.15) shows that there is good agreement between matlab and CST simulations also in this case. These figures show the electric farfield with and without compensating phase-shift, in comparison with the desired pattern of the linear array: applying the projection method, the pattern is partially recovered, especially in the main lobe direction, but again from 90° to 180° the pattern can't be recovered in an equally effective way.

Figure(4.16) represents the synthesis of the study on this conformal array: its CST-simulated uncorrected E-pattern, the corrected one and the desired ideal one, i.e. that of the linear array.

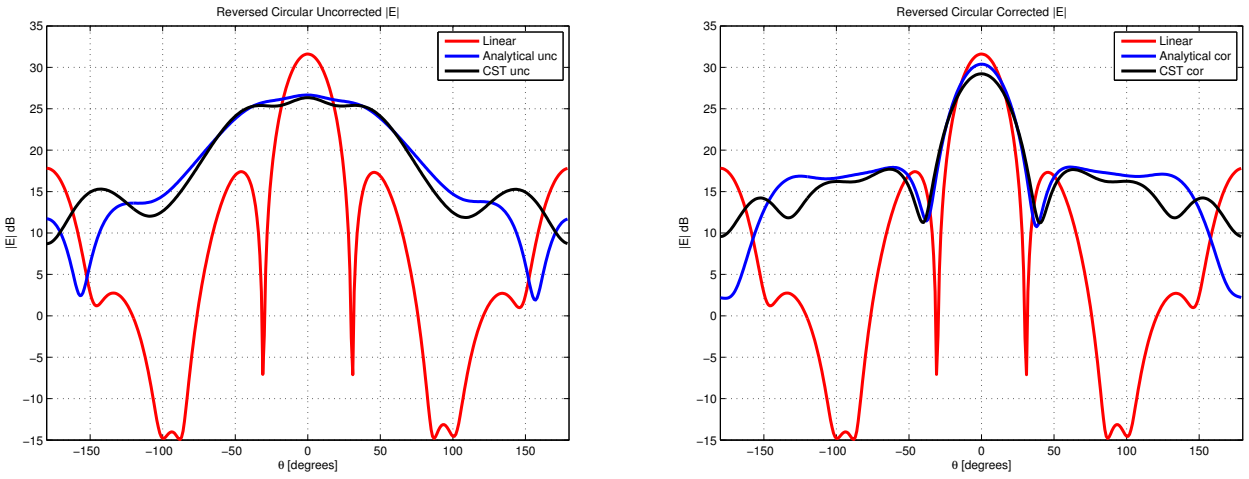

(a) Uncorrected.

(b) Corrected.

Figure 4.15: Analytical (matlab) in blue, simulated (CST) in black and desired (CST linear array) in red, E-field of the circular conformal array.

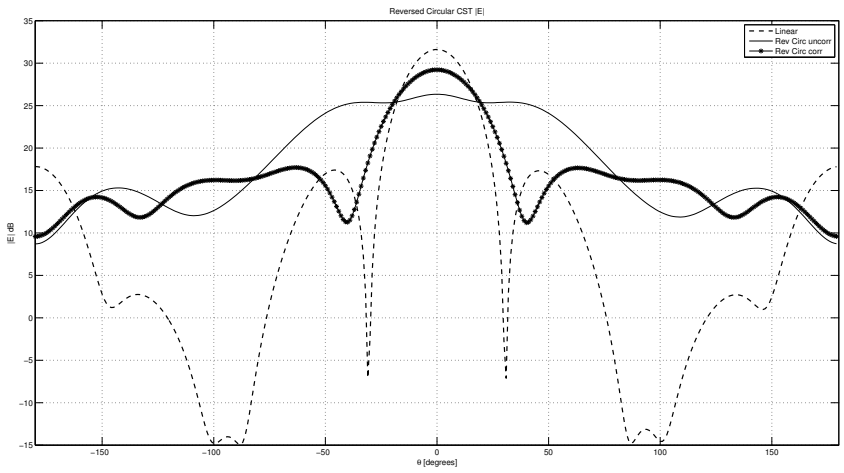

Figure 4.16: Circular array: CST-simulated E-field. Linear array (dashed line), circular uncorrected (plain) and corrected (marked).

Therefore we can conclude that the projection method works fine as a pattern recovery technique but it also shows some limitations: it enables

pattern recovery in the main lobe direction but its recovery capability decreases as soon as directions distant from broadside are considered. Again this is a consequence of the exisiting tradeoff for the projection method between ease of implementation and effectiveness.

4.4 *S*-Shaped Conformal Array

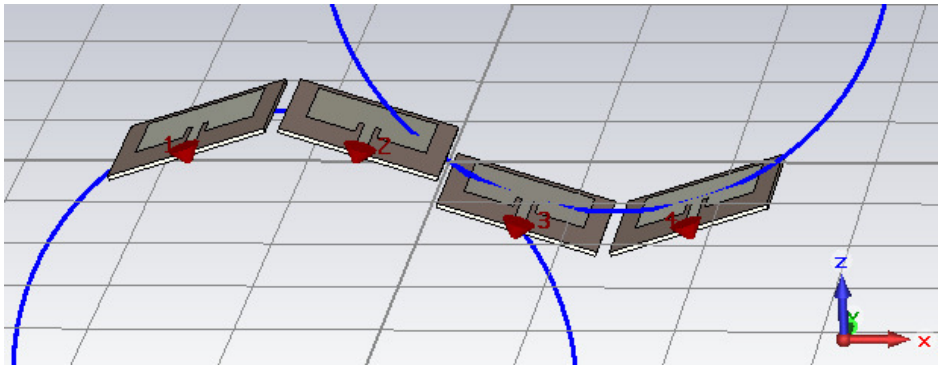

Figure 4.17: CST design of the *S*-shaped conformal array.

The two previous conformal arrays were used to build another geometry that comprises both the concave and convex circular arrays. In this case the 4-elements linear array is bent on a surface shaped as an S, as it's represented in Fig.(4.17) and described in detail in Section(1.5).

Fig(4.18) on the left represents the gain of the array when no pattern-recovery technique is adopted: it can be seen how the main lobe direction has changed from $0°$ to $9°$ and how the side lobe level has consistently increased from $-13.8\,dB$ to $-6\,dB$. The angular width and the maximum gain are instead only slightly different from the ones of the linear array: $25.8°$ vs $24.6°$ and $10.5\,dB$ vs $11.1\,dB$.

The array's gain after the introduction of the compensating phase-shift is

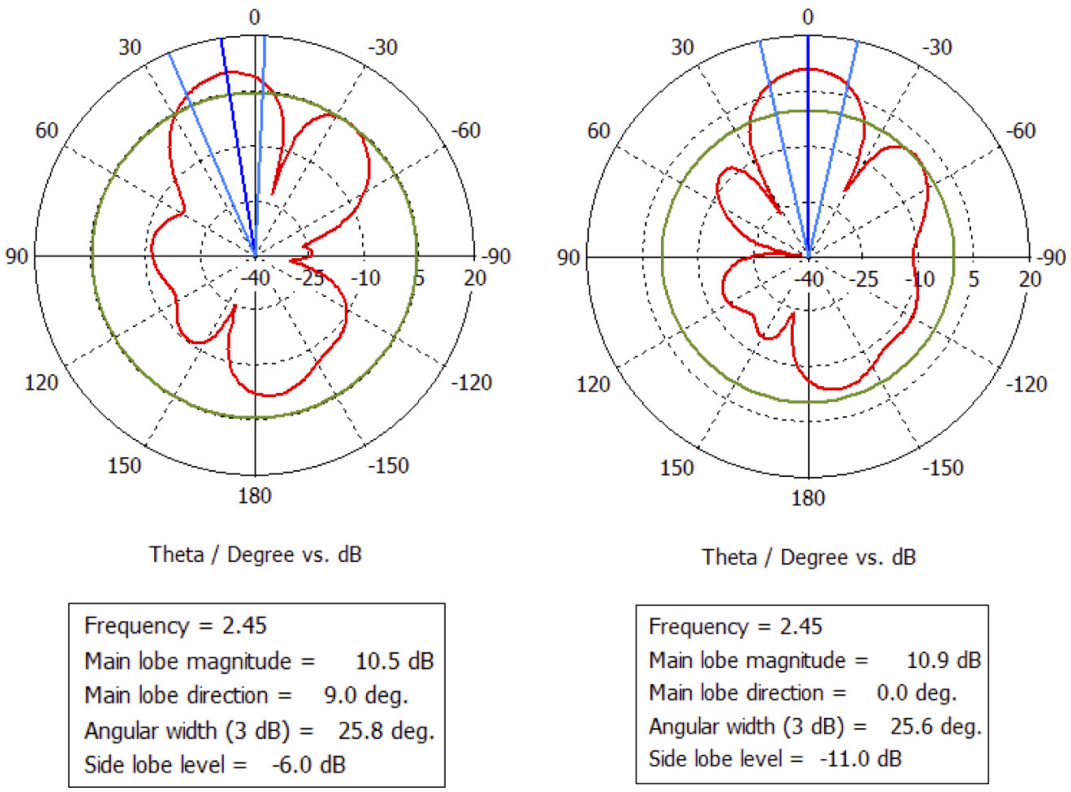

Figure 4.18: Polar plot of the array gain for the uncorrected (left) and corrected (right) cases (S shaped array).

reported in the right-most part of Fig.(4.18): the main lobe direction moves back to 0°, and the side-lobe level decreases to $-11\,dB$.

Again there is good agreement between matlab and CST simulations as it's reported in Figure(4.19). The two Figures show the electric farfield with and without compensating phase-shift, in comparison with the desired pattern of the linear array: applying the projection method the pattern is partially recovered, especially in the main lobe direction, but again from 90° to 180° the pattern can't be recovered in an equally effective way.

In Figure(4.20) the CST-simulated uncorrected E-pattern, the corrected one and the linear array's one are represented.

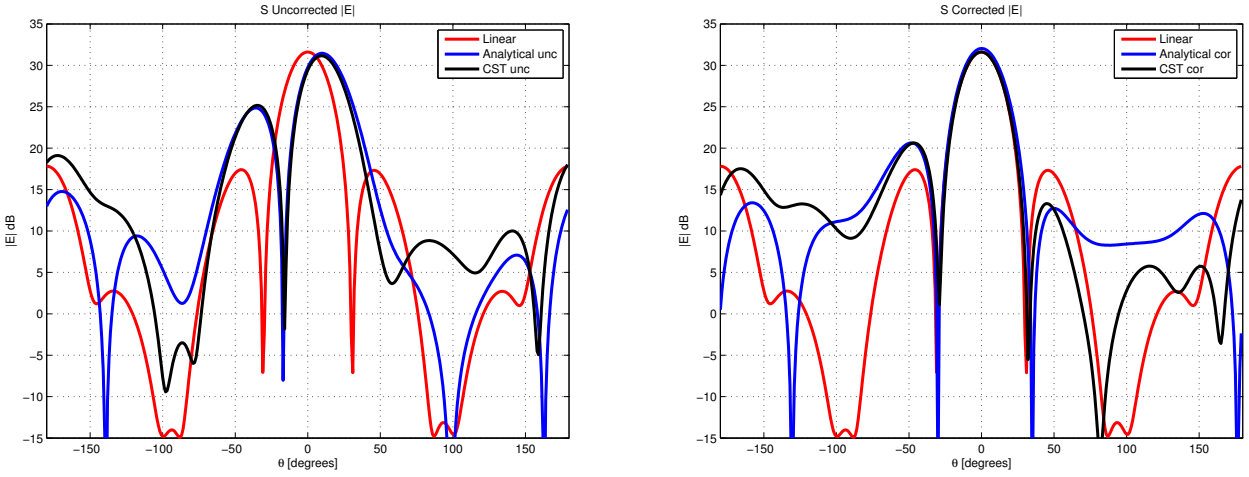

(a) Uncorrected.

(b) Corrected.

Figure 4.19: Analytical (matlab) in blue, simulated (CST) in black and desired (CST linear array) in red, E-field of the S conformal array.

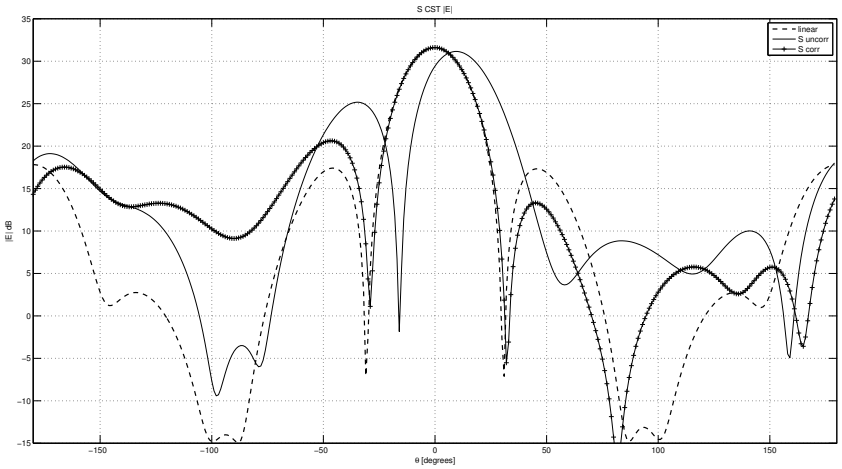

Figure 4.20: S array: CST-simulated E-field. Linear array (dashed line), uncorrected (plain) and corrected (marked).

Again the advantages and limitations of the projection method can be observed. In this case, performance degradation is not as much emphasized as in the previous cases: this can be explained observing that, among all the

conformal arrays presented so far, this is the most similar one to the linear array. Infact the patch antennas are only slightly rotated around their axis and the required phase-shift is smaller than in the previous cases (79.5° vs 101.8°).

4.5 Wedge Conformal Arrays

Another group of conformal arrays studied in this work comprises those obtained bending the 4-elements linear array on a wedge surface. In particular, three arrays of this type were studied and are represented in Figure(4.21): a conformal array bent of an angle $\vartheta_b = 30°$, its reversed version and another array bent of an angle $\vartheta = 45°$. The first and the last one were also physically realized and characterized at the North Dakota State University.

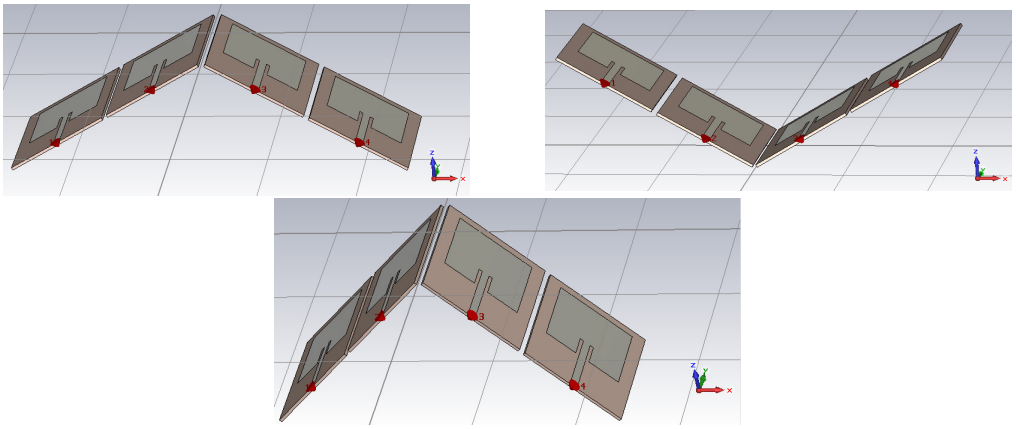

Figure 4.21: Different wedge conformal arrays.

Figures(4.22) report the gain patterns for the three arrays with and without the compensating phase-shift introduced with the projection method, while Table(4.2) contains the metrics and their respective values.

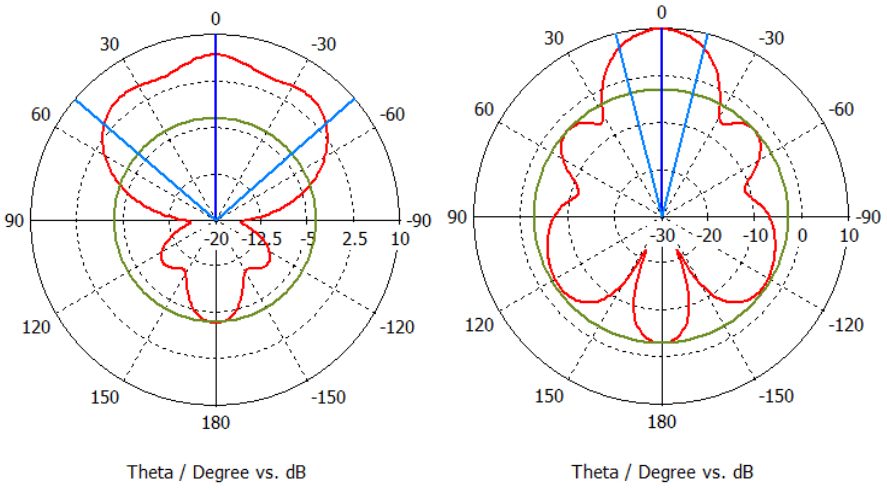

(a) 30° Uncorr.

(b) 30° Corr.

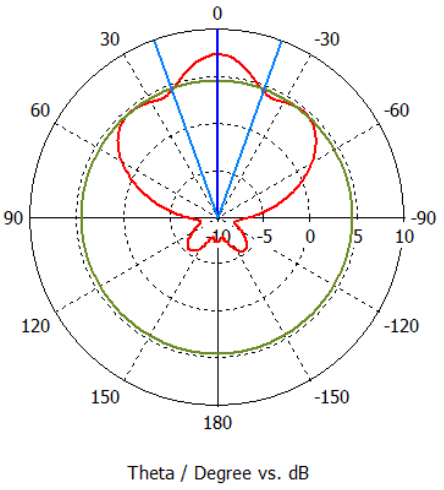

(c) 30° Rev. Uncorr.

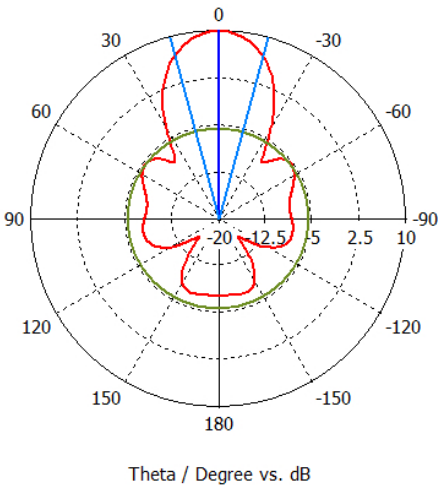

(d) 30° Rev. Corr.

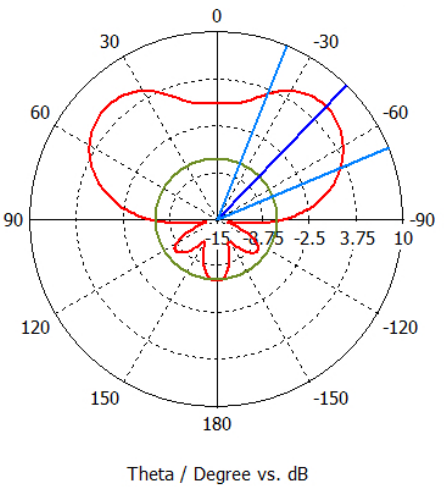

(e) 45° Uncorr.

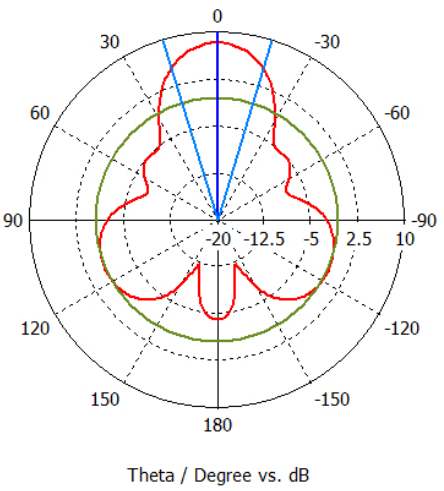

(f) 45° Corr.

Figure 4.22: Gain polar plot for the wedge conformal arrays.

From the figures and the table it can be easily seen that for all the three cases the performance downgrades with respect to the linear array: the main lobe magnitude decreases, the angular width and side lobe levels increases and, for $\vartheta = 45°$ even the main lobe direction changes.

Poor performance are much more evident when $\vartheta = 45°$: the greater ϑ, the more the conformal array is different from the linear one, i.e. the more the patches's main lobe direction points away from broadside. Moreover, as ϑ increases from 0° to 90°, the antenna become closer and closer, thus enhancing the effects of mutual coupling. This is evident also when the compensating phase-shift is introduced: it can effectively correct the main lobe magnitude and direction together with its angular width, but it has no effect on the side lobe level that, instead of decreasing, slightly increases.

When $\vartheta = 30°$ instead, the projection method is effective on all the metrics of interest as it can be seen by Table(4.2); infact for both the concave and convex array configurations all the metrics improve after the introduction of the compensating phase-shift.

As far as these arrays are concerned, similar considerations to those made for the concave and convex circular ones hold: in the concave array the maxima of the antennas are pointing away from broadside, i.e. away from the other elemets's radiating slots, while in the convex configuration the maxima of the antennas are pointing towards broadside, i.e. toward the othere elements's radiating slots. This fact comports a higher degree of mutual coupling between adjacent elements as it can be seen from the higher values of the parameters S_{21}, S_{32}, S_{43}:

Circular Array	S_{21} $[dB]$	S_{32} $[dB]$	S_{43} $[dB]$
Concave	-15	-24	-15
Convex	-14	-9	-14

in this case the parameters S_{21} and S_{43} don't change much, while S_{32} changes dramatically increasing of $15\,dB$ and becoming the highest of the three parameter in the convex configuration, while it was the lowest in the concave one.

This is intuitive if we consider that elements 2 and 3 (i.e. the central ones) are those that are more influenced by this surface change (from concave to convex): in the concave array their maxima were divergent with respect to each other, while they were parallel with respect to elements 1 and 4; in the convex array their maxima become convergent to each other while they keep being parallel to those of elements 1 and 4.

Therefore it can be seen how the mutual coupling level is higher in the convex configuration than in the concave one, thus bringing to slightly different results as far as the pattern-recovery capability of the projection method is concerned (see Table(4.2)).

		Uncorrected			Corrected		
Metrics	Linear	30°	30° Rev.	45°	30°	30° Rev.	45°
Main Lobe Mag. [dB]	11.1	6.76	7.35	6.02	9.92	9.99	8.37
Main Lobe Dir. [deg]	0	0	0	-44	0	0	0
Angular Width [deg]	24.6	98.2	39.7	45.2	28.3	30.1	33.4
Side Lobe Level [dB]	-13.8	-10.2	-2.8	-12.8	-12.8	-15.5	-8.9

Table 4.2: Metrics and correspondent values for the three wedge conformal arrays.

Also in this case there is a good match between analytical (matlab) and CST results as it is shown in Figure(4.23). Similar considerations to those made for the circular conformal arrays hold: from Figures(4.23) it can be seen how the action of the projection method is effective especially near the main lobe, while for $|\vartheta| \in [90°, 180°]$ the recovered pattern is pretty different from the desired one (i.e. the linear array pattern).

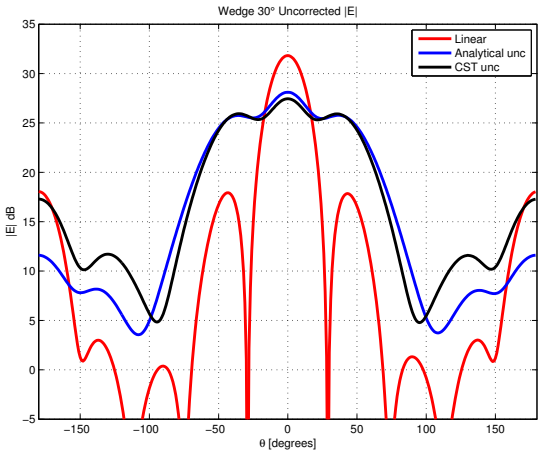

(a) 30° Uncorr.

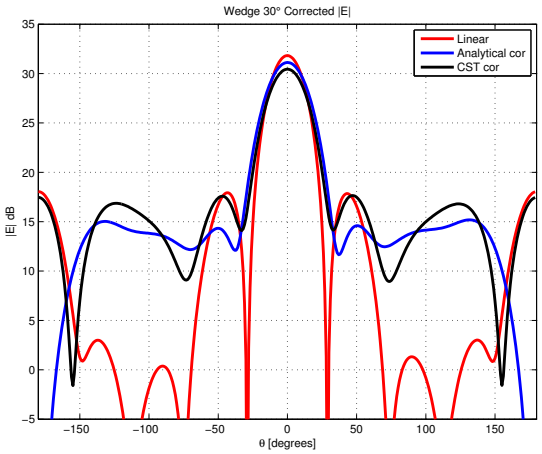

(b) 30° Corr.

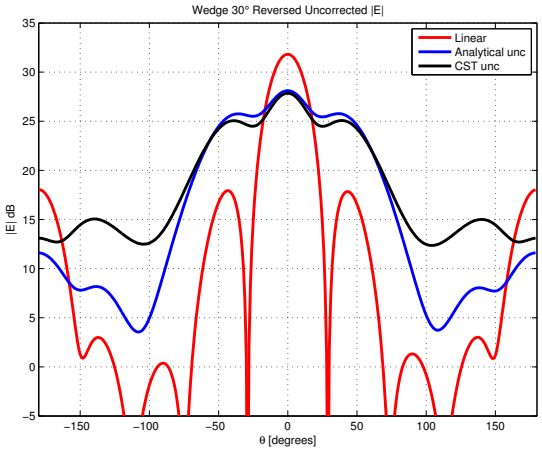

(c) 30° Rev. Uncorr.

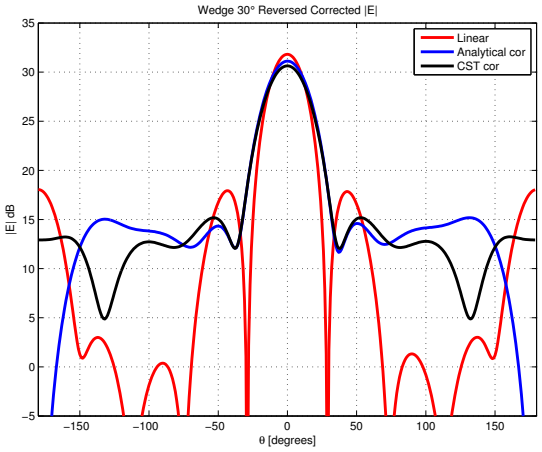

(d) 30° Rev. Corr.

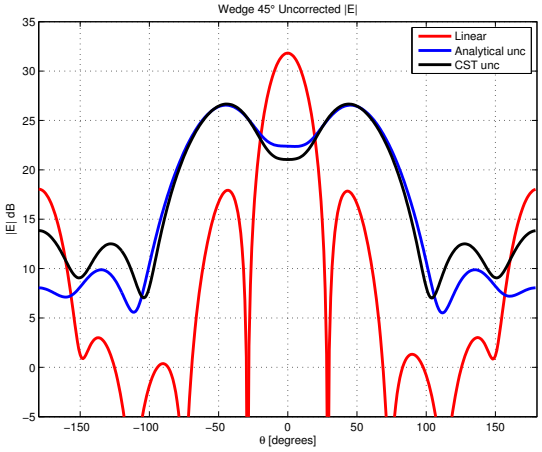

(e) 45° Uncorr.

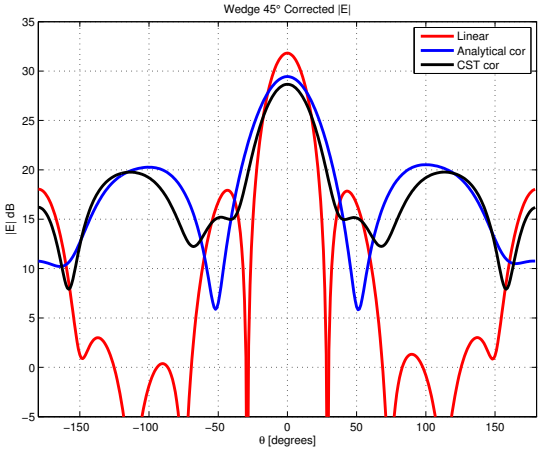

(f) 45° Corr.

Figure 4.23: Analytical (blue), simulated (black) and desired (red) E-field of the wedge conformal arrays.

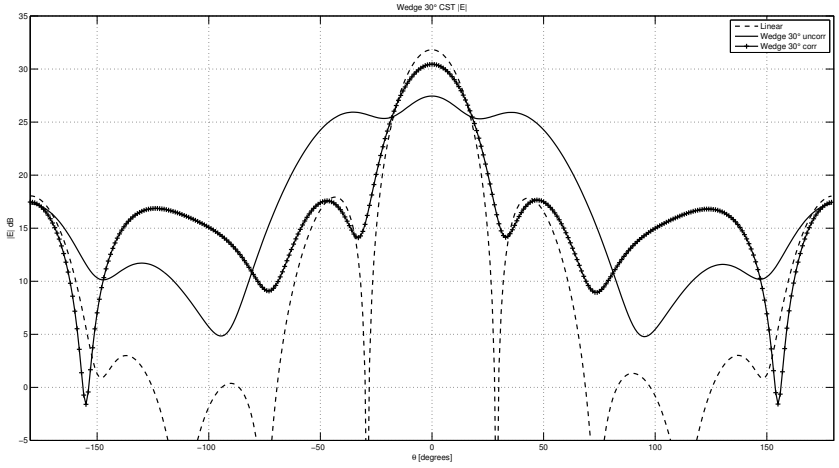

(a) $\vartheta = 30°$

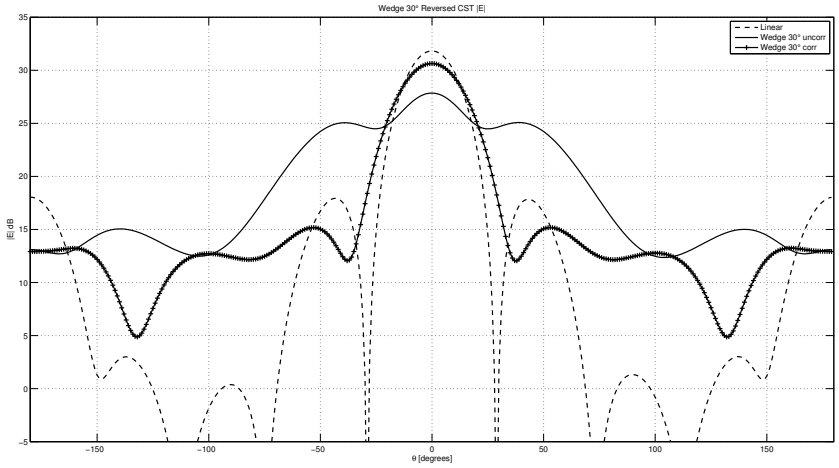

(b) $\vartheta = 30°$ Reversed.

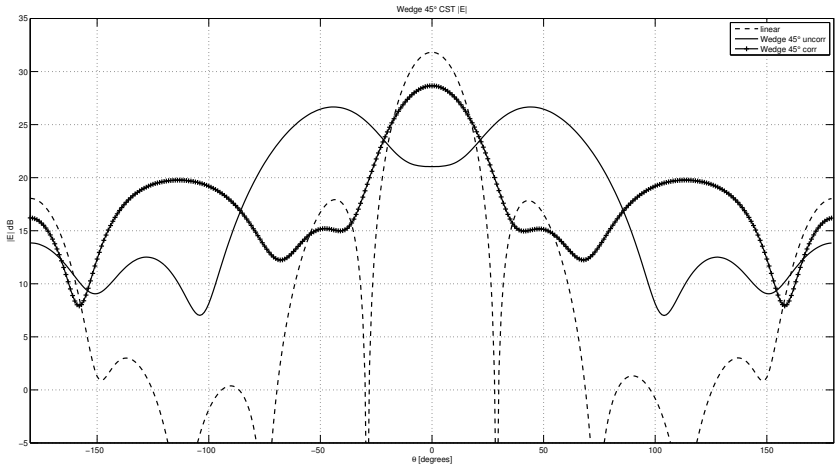

(c) $\vartheta = 45°$.

Figure 4.24: Wedge arrays: CST-simulated E-field. Linear array (dashed line), uncorrected (plain) and corrected (marked).

It can be also noticed again how the better results are obtained for $|\vartheta| = 30°$, while when $\vartheta = 45°$ the recovered pattern is less similar to the linear array's one even around the main lobe direction $\vartheta = 0°$.

Figures(4.24) show more directly the improvement brought by the introduction of the compensating phase-shift to each one of the wedge conformal arrays. It can be remarked again how the projection method is less effective far from boradside and for a higher angle ϑ.

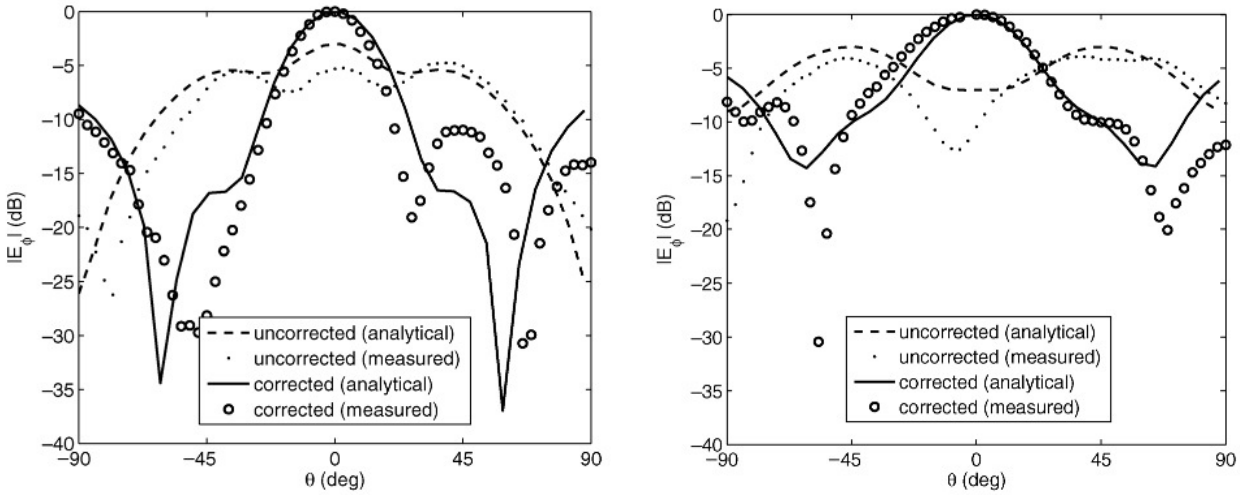

(a) $\vartheta = 30°$.

(b) $\vartheta = 45°$.

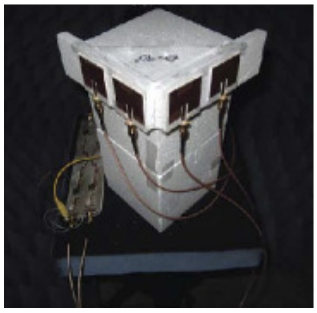

(c) Prototype.

Figure 4.25: Analytitcal and measured results in [19] and picture of the prototype of a wedge array.

Finally, Figure(4.25) reports an image of the prototype of the conformal

array attached to a nonconducting wedge together with the analytical and measured results obtained for $\vartheta = 30°, 45°$ at the North Dakota State University: these results agree with those obtained in this work[4].

4.6 Z-Shaped Conformal Array

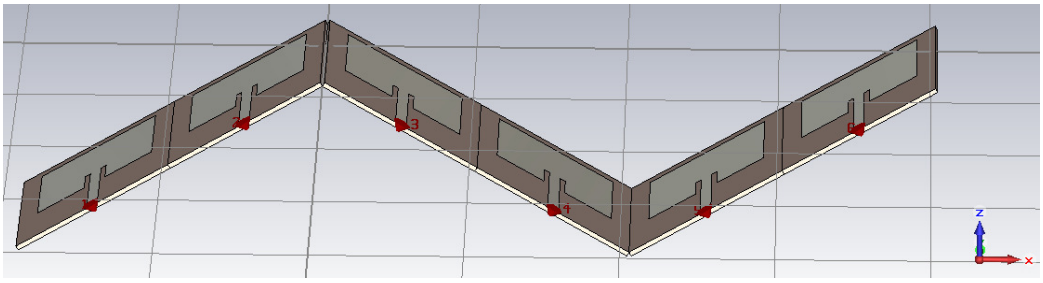

Figure 4.26: CST design of the Z conformal array.

The last conformal array that has been studied in this work derives from a six-elements linear array bent along a Z-shaped surface, as represented in Figure(4.26).

The CST and matlab implementation's procedure is the same as in all the previous cases. The main difference in this configuration is that the array is formed by six antennas instead of four, and so all the comparisons and cosiderations have to be made with respect to the original unbent 6-elements linear array, whose polar gain pattern is represented in Figure(4.27). It can be noticed that the main lobe magnitude of the linear array is now greater than the one of the 4-elements array and almost six times the one of the single patch antenna, as it was expected. Also the main lobe's angular width is lower in this case since the higher the number of elements of the linear

[4]It must be considered that in Fig.(4.25) ϑ is limited in the range $[-90°, 90°]$ (instead of the full range $[-180°, 180°]$ of Fig.(4.24)) and that the E-field is depicted in a relative scale.

array, the higher the directivity.

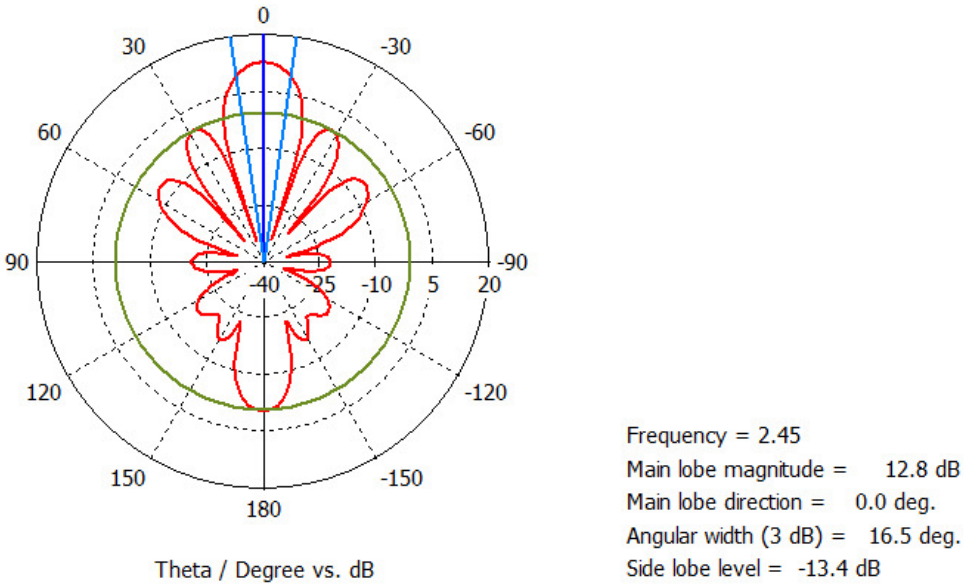

Figure 4.27: Gain's polar plot of the 6-elements linear array.

Figures(4.28) show the polar plot of the Z-shaped array without and with phase-compensation. If no pattern-recovery technique is applied, the characteristics of the array change:, the main lobe magnitude decreases, the angular width increases, the side lobe level decreases to $-7.4\,dB$ and above all, a grating lobe appears approximately in the direction $\vartheta = -35°$.

The main benefit of the projection method is the removal of the grating lobe. As far as the other metrics are concerned, similar considerations to the previous cases apply: the main lobe magnitude increases, the angular width decreases as the side lobe level.

Moreover from Figures(4.29) it can be seen that even in this case there is a good match between CST and matlab simulations.

Finally Fig.(4.30) represents the CST simulated uncompensated and compensated E-field together with the linear array's one: once more it can

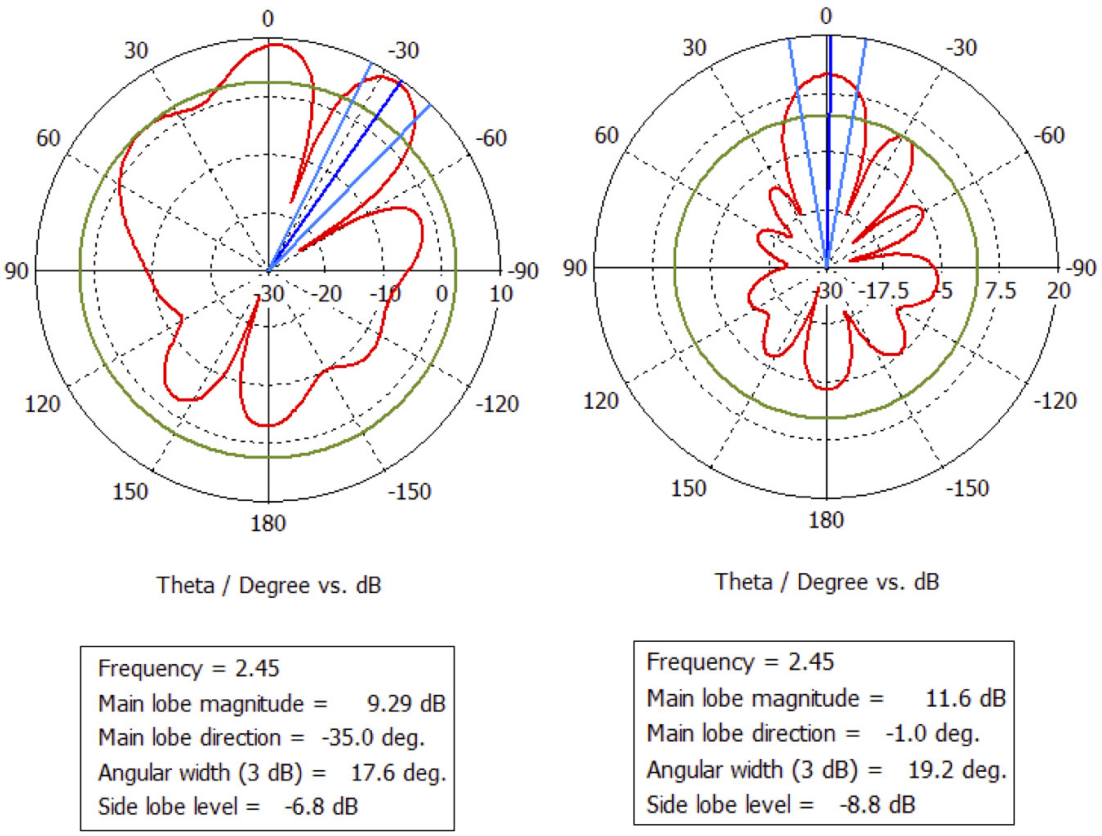

Figure 4.28: Polar plot of the array gain for the uncorrected (left) and corrected (right) cases (Z array).

be remarked that the projection method is effective as a pattern recovery technique especially around the main lobe's direction. When ϑ approaches angles wider than 90° the recovery-capability of the projection method is not as effective as in the proximity of the main lobe. Again, this can be pointed out as a limit of the projection method but, as it has been said several times, this is a consequence of the tradeoff between ease of implementation and performance. More complex and more accurate pattern recovery techniques could be used, but at the expense of a more complex control system, that for some applications is not feasible.

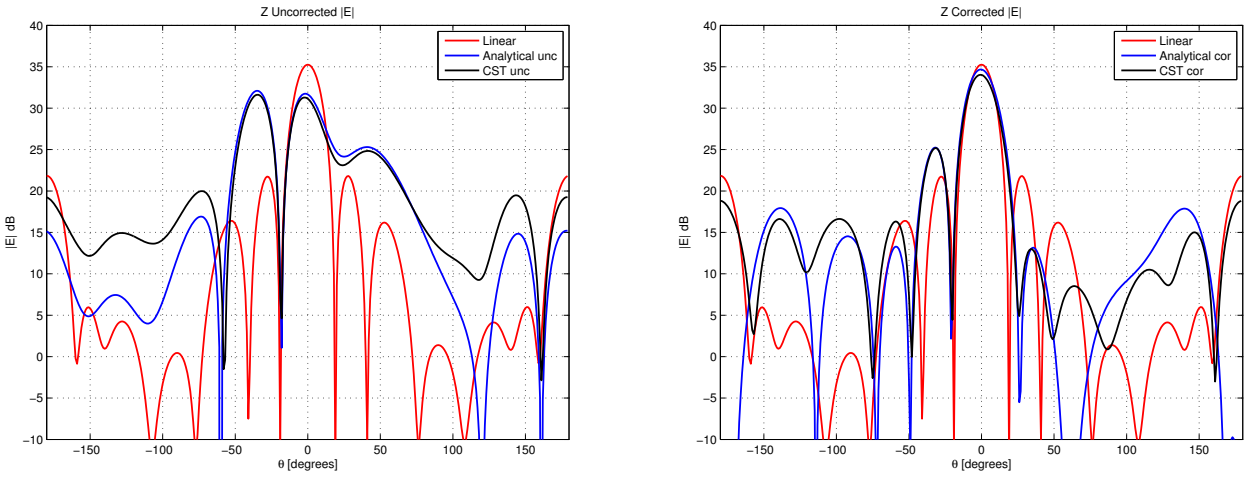

(a) Uncorrected.

(b) Corrected.

Figure 4.29: Analytical (matlab) in blue, simulated (CST) in black and desired (CST linear array) in red, E-field of the Z conformal array.

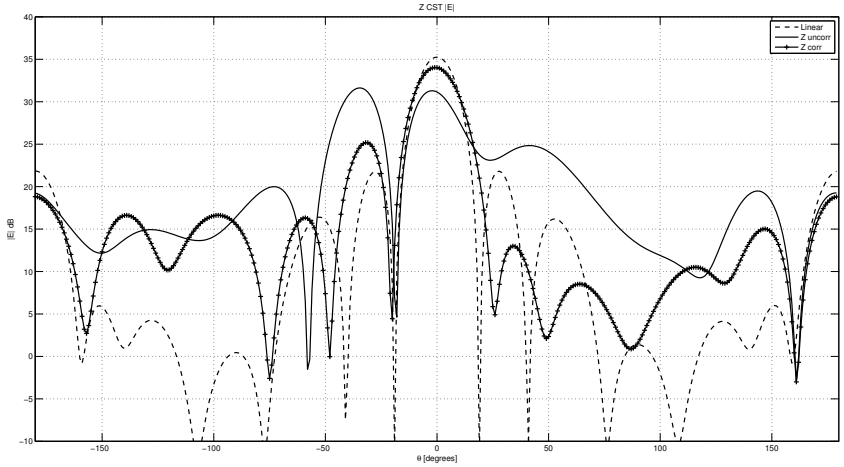

Figure 4.30: Z array: CST-simulated E-field. Linear array (dashed line), circular uncorrected (plain) and corrected (marked).

Chapter 5

Conclusion and Future Work

In this work various conformal arrays have been studied. Conformal arrays change shape in time in order to adapt to surfaces whose shapes vary as well: these arrays are designed in order to satisfy specific performance requirements when their geometry is fixed, but also to match some of these features when their shape changes.

The aim of this thesis was to analyze how the characteristics of these arrays changed when the arrays deformed, and to compare these performance with those obtained exploiting the projection method as a pattern recovery technique.

All the analyzed array geometries were obtained as different deformations of a linear array (composed by 4 or 6 elements). Some of these geometries were studied also in other works (e.g. [19]), namely the concave circular array and the ones placed on the two wedge surfaces bent of angles $\vartheta = 30^\circ\,,\ 45^\circ$; the other conformal arrays instead (the convex circular and wedge ones and the S and Z -shaped ones) are analyzed just in this work, providing an original contribution to this thesis.

The results presented in Chapter(1) can be summarized as follows:

1. The projection method provides a valid pattern recovery technique. The introduction of a proper phase-shift allows surface deformation's compensation, thus improving array performance: the main lobe gain increases and can be considered totally recovered as well as side lobe levels and angular width decrease, and the maximum direction is restored (if it had changed).

2. The correcting capability of the projection method depends on the conformal surface characteristics: as it was shown analyzing the two wedge-shaped conformal arrays bent of angles $\vartheta = 30°\,,\ 45°$, the more the surface is deformed, i.e. the more it is different from the original one, the less effective is the action of the projection method. This is confirmed also by the analysis of more complex conformal arrays like the Z-shaped one: as it was shown in the last section of Chapter(1), the compensating phase-shift is less effective with respect to the other (simpler) geometries.

3. The compensating phase-shifts are effective especially if performance enhancement around the main beam is considered. This can be easily explained considering that the projection method assumes that the main cause of poor performance is to be found in the phase difference among the signals, emitted by the array elements, when they reach a farfield observation point in the main lobe direction of the array. This explains the projection of the array elements onto the plane perpendicular to the main lobe direction and therefore clarifies why performance enhancement is more evident around this direction.

4. The more the mutual coupling is negligible, the more the projection method is effective. This was shown comparing the concave and convex

configurations of the wedge and circular array: in the convex arrays the degree of mutual coupling among the elements is less negligible than in the concave geometries and infact, even if theoretically the results should be equal to those of the convex arrays, they aren't. The convex configurations show a less effective (even if just slightly) action of the projection method.

Therefore the projection method can be considered a valid pattern recovery technique, cheap and easy to implement (as it was shown in [19] since it can be realized using just a flexible resistive sensor and a phase-shifter). By the way, as stated above, it is also evident that this pattern recovery technique has some drawbacks; this is a consequence of the unavoidable tradeoff between implementation simplicity and performance enhancement.

The choice of this technique rather than more complex ones (e.g. those that require extensive digital-signal-processing computations and RF circuitry beyond phase- and amplitude- tapering devices) depends on the application's requirements: if low cost and ease of implementation are priorities, then the projection method represents a good solution for pattern recovery. These features are desirable for many applications, especially those related to simple systems for which more complex control techniques are not feasible (e.g. simple wearable devices).

Future Work

This thesis provides the basis for future developments, as for example the physical implementation and characterization of the prototypes of the original conformal geometries presented here (the convex circular and wedge arrays, the S- and the Z- shaped ones).

However the most interesting possible future development consists in the study, design and prototyping of an autonomous self-adapting auto-corrective system for conformal arrays that change shape in time. So far infact, the compensating phase-shifts based on the projection method, were theoretically calculated for this type of self-adapting conformal arrays, but they were implemented just for static conformal arrays, i.e. arrays that change shape from their original configuration to another specific one.
This is quite a great simplification, since in more realistic systems surface deformation is a continuous phenomenum: when a wearable device is placed on a moving body, its conformal array should be able to adapt to a constantly changing surface (e.g. an arm or a leg of a walking person).

In order to do this, a more coprehensive theoretical study about conformal arrays must be conducted: a general relation between surface deformations and radiation pattern changes should be derived in order to develop new pattern recovery techniques.
A more exhaustive theoretical approach would also enable to determine the limits of self-adapting conformal antennas in terms of efficiency, maximum surface deformation and maximum rate of deformation.

Bibliography

[1] Samsung. *5G Vision*. 2015. URL: http://www.samsung.com/global/business-images/insights/2015/Samsung-5G-Vision-0.pdf.

[2] Mérouane Debbah. *5G Vision*. 2015. URL: http://www.dei.unipd.it/~zorzi/5GPadovaDebbah.pdf.

[3] Huawei. *5G: A Technology Vision*. 2013. URL: http://www.huawei.com/5gwhitepaper/.

[4] Y. Rahmat-Samii. H. Hurme P. Salonen and M. Kivikoski. "Dualband Wearable Textile Antennas". In: *Proc. IEEE Antennas Prop. Soc. Int. Symp. Dig.* 1 (2004), pp. 463–466.

[5] M. Klemm and G. Troester. "Textile UWB Antennas for Wireless Body Area Networks". In: *IEEE Trans. Antennas Propag.* 54 (2006), pp. 3192–3197.

[6] R. Langley S. Zhuand. "Dualband Wearable Textile Antenna on an EBG Substrate". In: *IEEE Trans. Antennas Propag.* 57.4 (2009), pp. 926–935.

[7] T. Deloues P. Lacomme H. Schippers P. Knott and M. R. Scherbarth. "Vibrating Antennas and Compensation Techniques Research in

NATO/RTO/SET 0877RTG 50". In: *Proc. IEEE Aerosp. Conf.* (2007), pp. 1–13.

[8] Constantine A. Balanis. *Antenna Theory: Analysis and Design.* Hoboken, New Jersey: John Wiley and Sons, 2005, pp. 283–385, 811–883.

[9] "Special Issue on Conformal Arrays". In: *IEEE Transactions on Antennas and Propagation* AP-22.1 (1974).

[10] Patrik Persson Lars Josefsson. *Conformal Array Antenna Theory and Design.* USA: John Wiley and Sons, 2006, pp. 1–9.

[11] E.Lier D. Purdy J. Ashe. *System and Method for Efficiently Characterizing the Elements in an Array Antenna.* US Patent: 2002/0171583 A1. 2002.

[12] G. Spalluto H. Schippers and G. Vos. "Radiation Analysis of Conformal Phased Array Antennas on Distorted Structures". In: *12th International Conference on Antennas and Propagation (ICAP 2003)* (2003), pp. 160–163.

[13] Davies D. E. N. "Circular Arrays: Their Properties and Potential Applications". In: *IEEE Proceedings of 2nd International Conference on Antennas and Propagation* (1981), pp. 1–10.

[14] Knudsen H. L. "The Field Radiated by a Ring Quasi-Array of an Infinite Number of Tangential or Radial Dipoles". In: *Proceedings of IRE* 41.6 (1953), pp. 781–789.

[15] A.; Mendoza-Radal A.; Roy S.; Ullah I.; Reich M.T.; Dawn D.; Braaten B.D.; Chamberlain N.F.; Anagnostou D.E. Ijaz B.; Sanyal. "Gain limits of phase compensated conformal antenna arrays on non-conducting spherical surfaces using the projection method". In: *IEEE International*

Conference on Wireless for Space and Extreme Environments (WiSEE) (2013), pp. 1–6.

[16] I.; Naqvi-S.A.; Ijaz B.; Masud M.M.; Booth B.; Asirvatham K.; Braaten B.D. Nariyal S.; Ullah. "On the use of amplitude tapering for pattern correction of conformal (Curved) antennas". In: *IEEE International Conference on Wireless for Space and Extreme Environments (WiSEE)* (2013), pp. 1–2.

[17] S.; Irfanullah; Nariyal S.; Anagnostou D.E. Braaten B.D.; Roy. "An autonomous self-adapting conformal array for cylindrical surfaces with a changing radius". In: *IEEE Antennas and Propagation Society International Symposium (APSURSI)* (2014), pp. 1784–1785.

[18] S. Sato I. Chiba K. Hariu and S. Mano. "A Projection Method Providing Low Sidelobe Pattern in Conformal Array Antennas". In: *IEEE Antennas Propag. Soc. Int. Symp. Dig.* (1989), pp. 130–133.

[19] S. Roy S. Nariyal I. Irfanullah N.F. Chamberlain M. T. Reich B.D. Braaten M. A. Aziz and D. E. Anagnostou. "A Self-Adapting Flexible (SELFLEX) Antenna Array for Changing Conformal Surface Applications". In: *IEEE Trans. Antennas and Propag.* 61.2 (2013), pp. 655–665.

[20] R.L. Haupt. *Antenna Arrays: a Computational Approach*. Hoboken, New Jersey, USA: John Wiley and Sons, 2010.

[21] Irfan Ullah and Benjamin D. Braaten. "Nulls of a Conformal Beamforming Array on an Arbitrary Wedge-Shaped Surface". In: *IEEE Antennas and Propagation Society International Symposium (APSURSI)* (2014).

[22] Irfan Ullah and Benjamin D. Braaten. "On the Effects of a Changing Cylindrical Surface on the Nulls of a Conformal Beamforming Array." In: *IEEE Antennas and Propagation Society International Symposium (APSURSI)* (2014).

[23] Lal Chand Godara. *Handbook of Antennas in Wireless Communications*. CRC Press, 2001, Chapter 6.

[24] E. O. Hammerstad. "Equations for Microstrip Circuit Design". In: *Proc. Fifth European Microwave Conf.* (1975), pp. 268–272.

[25] I.J. Bahl and P. Bhartia. *Microstrip Antennas*. Dedham, MA: Artech House, 1980.